

# **Determination of Stellar Parameters of the Eclipsing Contact Binary System S Ant using UBV Photometry and Spectroscopy**

By

Nipuni Palliyaguru

Dissertation submitted in partial fulfillment of the requirements for the  
**BACHELOR OF SCIENCE SPECIAL DEGREE IN PHYSICS**

Of the

**UNIVERSITY OF COLOMBO**

**SRI LANKA**

(June 2007)

## **DECLARATION**

I certify that this dissertation does not incorporate without acknowledgement, any material previously submitted for a Degree or Diploma in any University and to the best of my knowledge and belief it does not contain any material previously published or written or orally communicated by another person except where due Reference is made in the text.

.....  
Nipuni Palliyaguru

10.08.2007

## **ACKNOWLEDGEMENTS**

I wish to thank my project supervisor Dr. Chandana Jayaratne for granting me this research opportunity and also for his guidance throughout the project. I also wish to extend my gratitude to Dr. J.K.D.S Jayanetti, Head of the Department of Physics and all the academic staff members for their support.

I also wish to thank the director of the Arthur C. Clarke Institute for Modern Technologies (ACCIMT), Dr. Namasivayam for granting me permission to carry out the project at the astronomical Observatory of ACCIMT.

I am especially grateful to research scientists Mr. Sarajh Gunasekara, head of the Space Application division and Mr. Janaka Adassuriya of ACCIMT for their generosity and careful guidance throughout the project.

I also wish to thank research scientists Mr. Indika Medagangoda, Mr. Jayathu Fernando and other staff members of the space application division of ACCIMT for their invaluable support.

I have been fortunate to receive such good support from my family and friends who contributed in many ways.

## ABSTRACT

Spectrometric and photometric studies are used comprehensively by researchers in other countries to gather information on Binary stars. However research in this field is still developing in Sri Lanka due to the limited facilities available. This research on S Ant is the first attempt performed in Sri Lanka to obtain the velocity curve for a binary system using spectroscopic data. S Ant has rarely been subject to observation even in other countries which makes this study quite valuable.

The spectrum is a powerful type of data in the study of binaries. They emit spectra with absorption lines due to the elements present in their atmosphere.  $H\alpha$  and other metallic lines such as Fe and Mg are some of the prominent absorption lines. The research is very subtle since amazing facts about these distant binaries can be obtained simply by referring to the Doppler shift present in the spectral line.

The study was conducted at Arthur C. Clarke Institute for Modern Technologies (ACCIMT) situated in Moratuwa. Absorption line spectra of S Ant (HD 82610,  $m_v = 6.4$ ) were obtained during the period of January through May in 2007 in order to cover all phases of the orbit. Spectrograph with SBIG ST7 CCD Camera attached to the 45 cm Cassagrain telescope was used to obtain the spectra. A reflective grating with the dispersion element of 1200 lines/mm was used. Data reduction was done using the Linux based software, IRAF (Image Reduction and Analysis facility). Velocities of each primary and secondary component of the binary system were separately obtained for each phase using IRAF.

Results indicate that the velocities of the primary and secondary components are fitted with a sin curve and the peak velocities of 89.261 km/s and 208.589 km/s respectively. The spectroscopic mass ratio is therefore 0.42. This is in agreement with the results of the study "Radial Velocity Studies of Southern Close Binary Stars. II. Spring/Summer Systems I" by Rucinski and Duerbeck conducted in 2006.

# Content

## 1 Introduction

1.1 Spectroscopy fundamentals .....	1
1.2 Photometry fundamentals.....	1
1.3 Objective of the project and project environment.....	2

## 2 Literature survey

2.1 Binary Stars.....	3
2.1.1 History and significance of binary stars.....	3
2.1.2 Birth and evolution.....	3
2.1.3 Types of Binaries.....	4
2.2 S Ant.....	7
2.2.1 Historical Background.....	7
2.3 Absorption Line Profiles.....	7

## 3 Theory

3.1 Mechanics of a Binary system.....	8
3.1.1 Orbital orientation in binary systems.....	8
3.1.2 Laws governing the motion.....	9
3.2 Dopplers effect.....	10
3.3 Velocity curve of spectroscopic binaries.....	10
3.4 Light curve of eclipsing Binaries.....	12

## 4 Instrumentation

4.1 45 cm Cassagrain Telescope.....	14
4.2 Spectrograph.....	15
4.3 CCD Camera.....	16
4.3.1 Function of the CCD Camera.....	16
4.3.2 Quantum Efficiency of the CCD.....	16
4.3.3 Dark Current.....	17

4.3.4	Readout noise.....	17
4.3.5	CCD Cooling.....	17
4.4	12'' Caasegrain telescope.....	18
4.5	Photoelectric Photometer.....	18

## **5 Experimental Procedure**

5.1	Observation of Line Spectra.....	20
5.2	Observation Techniques in Photometry.....	22
5.2.1	Differential Photometry.....	22

## **6 Data Analysis and Results**

6.1	Data Reduction Procedure.....	23
6.2	Results.....	30
6.3	Velocity Curve of S Ant.....	34
6.4	Photometric data.....	38
6.5	Calculations.....	39

## **7 Discussion and Conclusion**

References.....	43
-----------------	----

## **Appendix**

Phase calculations.....	44
Error Calculations.....	46

## CHAPTER 1

# INTRODUCTION

---

Electromagnetic radiation emitted from stellar objects is currently the only source of information available, to investigate their characteristics. This radiation falls throughout the electromagnetic spectrum. This radiation can be studied in both spectroscopy and photometry.

### 1.1 Spectroscopy fundamentals

Stars can be classified spectrally into the well known OBAFGKM groups. Most stars emit a continuum of wavelengths with a number of absorption lines superimposed on it. The very hot O, B type stars have few features in their spectrum, perhaps only a few hydrogen lines. The cool K, M type stars tend to be old, with many metallic lines producing a very complex and structured spectrum.

A spectrograph is a device that can produce a graph of the intensity of light as a function of color, or wavelength. A detailed study of spectral lines of a star can lead way to find out information on stellar parameters such as its rotational velocity, temperature, pressure magnetic and electric field strengths.

### 1.2 Photometry fundamentals

The science of measuring the flux or the intensity of an astronomical object's electromagnetic radiation is called photometry. Usually it refers to measurements over a large wavelength bands of radiation. Photometry is generally used to generate light curves of objects such as variable stars and supernovae in which the total light energy output varies over time. By observing an object's light output over a period of time, deviations can be examined and possible causes for such deviations can be determined.

A photoelectric photometer measures the light intensity of an object by directing its light onto a photomultiplier tube. Measurements of flux, when coupled with some estimate of the distance to an object provides information on the total energy output of the object, its size and other physical properties like temperature. Accurate photometry is more difficult when the apparent brightness of the object is fainter.

### **1.3 Objective of the project and the project environment**

The Primary objective of this research is to determine the spectroscopic mass ratio of the eclipsing contact binary system S Ant. In order to determine the stellar parameters this system has to be studied both in photometry and spectroscopy. Spectroscopic data is used to calculate the spectroscopic mass ratio and Photometric data provides the period of the binary system. Individual masses of the binary system can be calculated by combining these two studies.

This system has not been subject to frequent observation and only a very few studies have been conducted by researchers in other countries. Therefore, the quality of our observations here in Sri Lanka can be compared with that of international laboratories, while contributing to fill the scarcity of observational data on this contact binary system.

This project was carried out under the guidance of scientists at the Arthur C. Clarke Institute for Modern Technologies (ACCIMT) at Katubedda, Moratuwa. Being situated in a large conurbation, the present telescope site suffers severe light pollution and poor sky conditions. Under these sky conditions, it is not feasible to carry out serious astronomy research with this telescope. Severe light pollution in the telescope site limit the visual magnitude of the telescope to 12 otherwise it could have been closer to its theoretical visual magnitude, 15. As an alternative to these issues ACCIMT has a 12” Schmidt Cassegrain portable telescope with a photometer which can be transported to remote locations where there is minimal light pollution, to collect photometric data.

## CHAPTER 2

# LITERATURE SERVEY

---

## 2.1 Binary Stars

### 2.1.1 History and significance of Binary stars

A binary star is a stellar system consisting of two stars orbiting around their center of mass. For each star, the other is its companion star. A true binary is bound together by gravity.

Close pairings of stars in the sky have been recognized since antiquity, but most people thought they were just chance superpositions along the line of sight of two unrelated stars. In 1767 the English clergyman John Michell realized that there are too many doubles to be explained by chance and that in many cases the two stars must actually be physically associated. In 1803, William Herschel discovered the first binary star - Castor in Gemini. By 1821, he had completed the first major catalogue of binaries, which contained 848 stars. Today, over a hundred thousand binaries are known. In 1991 and 1992, observing teams led by Michel Mayor and Geoffrey Marcy surveyed the stars in the solar neighborhood and concluded that nearly half of all stars are binary and most have highly eccentric orbits.

Because a large proportion of stars exist in binary systems, binaries are particularly important to our understanding of the processes by which stars form. In particular, the period and masses of the binary tell us about the amount of angular momentum in the system. Because this is a conserved quantity in physics, binaries give us important clues about the conditions under which the stars were formed. Binary stars also provide a unique laboratory for the study of matter under extreme physical conditions, pushing modern theories of physics, such as Quantum Mechanics and Einstein's General Theory of Relativity, to the limits of their predictive powers.

### 2.1.2 Birth and evolution

While it is not impossible that some binaries might be created through gravitational capture between two single stars, it has a very low likelihood. (Three objects are actually required, as conservation of energy rules out a single gravitating body capturing another) However when considering the high number of binaries, the process of gravitational capture cannot be the primary formation process.

The observation of binaries consisting of pre main sequence stars supports the theory that binaries are already formed during star formation. Computer simulations of the gravitational collapse of a molecular cloud indicate that if the cloud rotates faster than a critical rate of approximately one revolution every two million years, the cloud will

fragment into binary protostars with highly eccentric orbits. Therefore Fragmentation of the molecular cloud during the formation of protostars is an acceptable explanation for the formation of a binary or multiple star system.

The mass of a star determines how it will evolve and eventually die. In wide binaries, which typically have orbital periods of tens of years or more, the separation between the two stars is larger than the largest radius that either star will ever reach and hence the two stars will go through their entire life cycles independently. In close binaries (or interacting binaries), which have shorter orbital periods, a time will come when one star becomes a giant or super giant and fills its Roche lobe. There is then the possibility of mass transfer and completely new evolutionary paths are opened up for the two stars.

### **2.1.3 Types of binaries**

Binary stars are classified into four types *viz. visual, spectrometric, astrometric and eclipsing binaries* according to their observable properties. Any binary star can belong to several of these classes; for example, several spectroscopic binaries are also eclipsing binaries.

#### **2.1.3.1 Visual binaries**

A visual binary star is a binary star for which the angular separation between the two components is great enough to permit them to be observed as a double star in a telescope.

#### **2.1.3.2 Spectroscopic binaries**

A spectroscopic binary star is a binary star in which the separation between the stars is usually very small, and the orbital velocity very high. Unless the plane of the orbit happens to be perpendicular to the line of sight, the orbital velocities will have components in the line of sight and the observed radial velocity of the system will vary periodically. Since radial velocity can be measured with a spectrometer by observing the Doppler shift of the stars' spectral lines, the binaries detected in this manner are known as spectroscopic binaries. Most of these cannot be resolved as a visual binary, even with telescopes of the highest existing resolving power.

#### **2.1.3.3 Astrometric binaries**

An astrometric binary star is a binary star for which only one of the component stars can be visually observed. The visible star's position is carefully measured and detected to have a wobble, due to the gravitational influence from its counterpart.

### **2.1.3.4 Eclipsing binaries**

An eclipsing binary star is a binary star in which the orbit plane of the two stars lies so nearly in the line of sight of the observer that the components undergo mutual eclipses. In the case where the binary is also a spectroscopic binary and the parallax of the system is known, the binary is quite valuable for stellar analysis.

Eclipsing binaries are variable stars, not because the light of the individual components vary but because of the eclipses. The light curve of an eclipsing binary is characterized by periods of practically constant light, with periodic drops in intensity. If one of the stars is larger than the other, one will be obscured by a total eclipse while the other will be obscured by an annular eclipse.

**Another classification of binaries is based on the distance of the stars, relative to their sizes.**

#### **Detached binaries**

These are a kind of binary stars where each component is within its Roche lobe, i.e. the area where the gravitational pull of the star itself is larger than that of the other component. The stars have no major effect on each other, and essentially evolve separately. Most binaries belong to this class.

#### **Semidetached binary stars**

These are binary stars where one of the components fills the binary star's Roche lobe and the other does not. Gas from the surface of the Roche lobe filling component (donor) is transferred to the other star (accretor). The mass transfer dominates the evolution of the system. In many cases, the inflowing gas forms an accretion disc around the accretor. Examples of this type are X-ray binaries and Cataclysmic variable stars.

#### **Contact binary stars**

This is a type of binary star in which both components of the binary fill their Roche lobes. The uppermost part of the stellar atmospheres forms a common envelope that surrounds both stars. As the friction of the envelope breaks the orbital motion, the stars may eventually coalesce. Probably most Spectroscopic and eclipsing pairs are contact.

**The eclipsing binaries are also classified according to the ways the light changes occur.**

## Beta Lyra

These stars are not in physical contact but still a great deal of mass transfer takes place. The two components have unequal surface brightness. Therefore the light curve has two minimas of different depth as shown below.

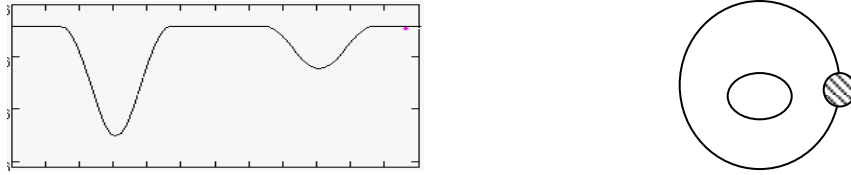


Fig. 2.1 The light curve and the relative orbit of a Beta Lyrae system

## Algol

The companion and primary stars are almost equal in size, but the luminosities are different. The light curve consists of two minimas of different depth.

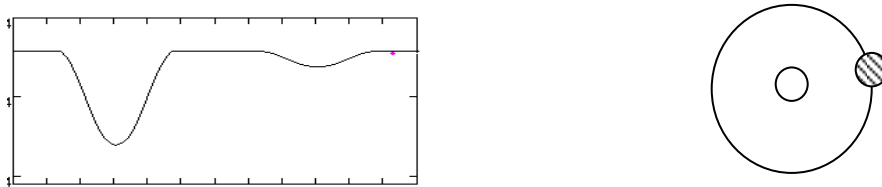


Fig. 2.2 The light curve and the relative orbit of an Algol system

## W Ursa Majoris

The companion touches the primary star leading to a great deal of mass transfer. The companions have identical brightness resulting in a light curve with minimas of approximately same depth.

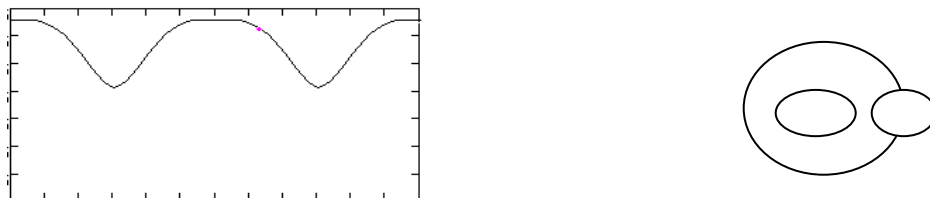


Fig. 2.3 The light curve and the relative orbit of a W UMa system

## 2.2 S Ant

The star S Ant is an eclipsing close binary system in the constellation Antilae . It is situated on the southern part of the celestial sphere with Right Ascension and Declination 09h 32m 18.40s,  $-28^{\circ} 37' 40.0''$  (EpoC 2000) respectively. It is a relatively bright double line spectroscopic binary system with the visual magnitude  $V_{\max} = 6.28$  and the spectral type of A8. Its companion star has a visual magnitude of 7 and spectral type of F. S Ant is a short period UMa type system with Period  $P = 0.6483$  days. Other names such as HD 82610, HIP 46810 and CD 287373 are also used to identify this system.

### 2.2.1 Historical background

The star has been studied recently under Slaveck Rucinski's publication, Radial Velocity Studies of Southern Close Binary Stars (2006). It was also studied under Determination of Parameters of W UMa systems by G. Ruso, C. Sollazo and L. Milano in 1981.

S Ant has been a frequent target of photometric observations, but the only previous spectroscopic observations were by Popper (1956) who saw only one component with  $K1 = 92.3 \pm 1.5 \text{ km s}^{-1}$  (Rucinski, 2006)

## 2.3 Absorption line Profiles

An absorption line is a dark line in an otherwise uniform and continuous spectrum, resulting from a deficiency of photons in a narrow frequency range, compared with the nearby frequencies. Absorption lines are produced when the emitted radiation is absorbed by the star's gaseous outer region, or atmosphere.

For a binary star, the spectral lines will be shifted from its original position due to Doppler Effect since it keeps orbiting around the center of mass.

It may also be broadened. Line broadening appears due to several reasons. One is *natural broadening*, which is always present. The Uncertainty principle relates the life of an excited state with the precision of the energy, so the same excited level will have slightly different energies, which is the reason for this. Also the individual hydrogen atoms are moving very fast due to the tremendous temperatures involved, producing *Doppler broadening* which result in a spread in the frequency of the observed line. Broadening can also occur due to rotations of the object, when the spectra include light from parts of the star that move towards and away from the observer.

## CHAPTER 3

### THEORY

---

#### 3.1 Mechanics of a binary system

##### 3.1.1 Orbital orientation in binary systems

Binary star systems can have different orientations of their orbital planes with respect to our line of sight, as illustrated in figure 3.1.

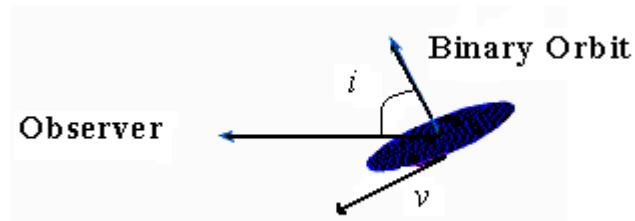


Fig. 3.1 Tilt of the orbit of a binary system

If  $i$ , the angle between the line of sight and the normal to the plane of binary system, is sufficiently close to 90 degrees, the two stars can eclipse each other when they revolve around their common center of mass, as seen by the observer on the earth.

##### 3.1.2 Laws governing the motion

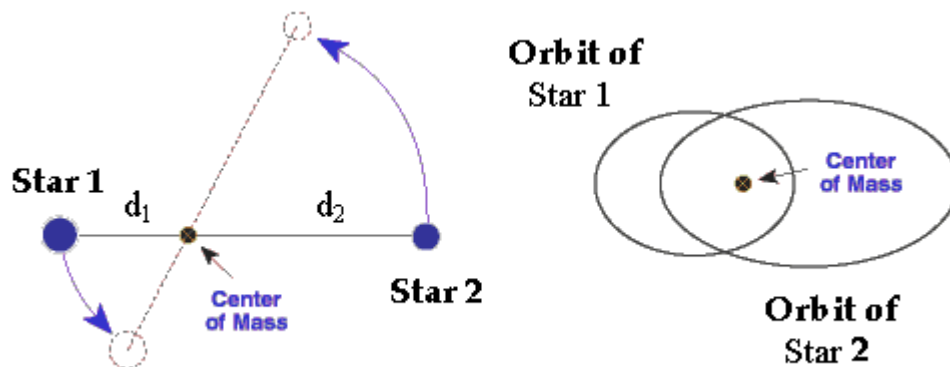


Fig. 3.2 In a binary system the two stars orbit their center of gravity.

- $M_1$  - mass of star 1
- $M_2$  - mass of star 2
- $d_1$  - distance to the star 1 from the center of gravity (orbital radius of star 1)
- $d_2$  - distance to the star 2 from the center of gravity (orbital radius of star 2)

By the definition of center of gravity,

$$M_1 d_1 = M_2 d_2 \dots\dots\dots 3.1$$

Due to the equilibrium between gravitational and centrifugal forces of a Binary system,

$$\frac{GM_1 M_2}{(d_1 + d_2)^2} = M_1 \omega_1^2 d_1$$

- $\omega_1$  - angular velocity of star 1
- $\omega_2$  - angular velocity of star 2
- $G$  - Gravitational constant

Center of gravity to remain at constant velocity  $\omega_1 = \omega_2 = \omega$

For circular orbits  $\omega_1 = \frac{2\pi}{T}$

T - orbital period

$$\frac{GM_1 M_2}{(d_1 + d_2)^2} = \frac{M_1 d_1 4\pi^2}{T^2} \dots\dots\dots 3.2$$

This yield,

$$d_1 + d_2 = d_1 + \frac{M_1 d_1}{M_2}$$

$$\frac{M_2}{d_1} = \frac{M_1 + M_2}{d_1 + d_2} \dots\dots\dots 3.3$$

Combining equations 3.2 and 3.3 yields the general form of Kepler's third law

$$M_1 + M_2 = \frac{4\pi^2 (d_1 + d_2)^3}{T^2 G} \dots\dots\dots 3.4$$

## 3.2 The Doppler Effect

Since the frequency of the light of the binary star system changes when the light source moves towards the earth or away from the earth, it causes a shift in frequency or wavelength.

If the light source moves towards the observer the wavelength becomes shorter by  $\Delta\lambda$  where,

$$\frac{\Delta\lambda}{\lambda_0} = \frac{V_r}{C}$$

$\lambda_0$  - Rest wavelength of the line (Wavelength of the line if the light source and the observer have the same velocity)

$v_r$  - Radial velocity

If the light source moves away from the earth, the wavelength becomes longer by the same relative amount. It is this wavelength shift, which permits to measure the radial velocities of the stars.



Fig. 3.3 The component of the velocity in the direction of the observer.

## 3.3 Velocity curve of spectroscopic binaries

Since Doppler shift is produced by the radial velocity, it is important to know how the radial velocity changes in relation to the orbital speed as a star revolves in its orbit, when viewed from different directions. Consider two stars revolving in circular orbits separated by a relatively small distance with different radii round the common center of mass (Figure 3.4).

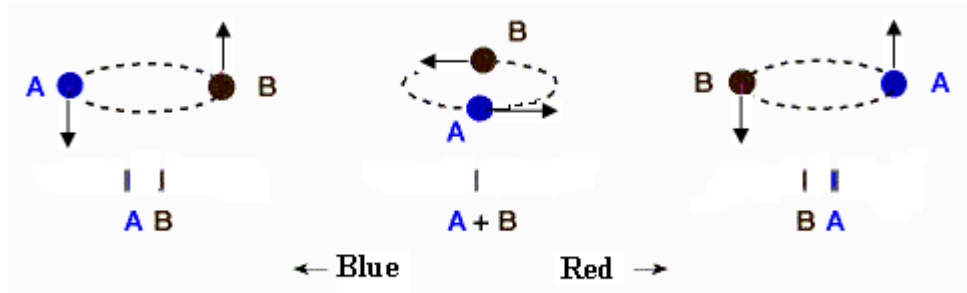


Fig. 3.4 Explanation of Spectral lines of a double spectroscopic binary system.

Because of the motion of the two stars around their common center of mass, each star is alternatively moving toward the observer and then away. But because of the Doppler Effect, this means that the spectral lines will periodically be shifted up and down in wavelength and that for the two stars this shift will be in the opposite direction: when star A is moving toward us, star B is moving away from us, and vice versa.

Thus, the motion toward the observer gives a blue shift (negative velocity) while motion away from the observer gives a red shift (positive velocity). For example, at position 1 (figure 3.5) the red star has maximal velocity away from the observer and the blue star has maximal velocity toward the observer, while at position 2 the radial velocity of each star relative to the observer is zero.

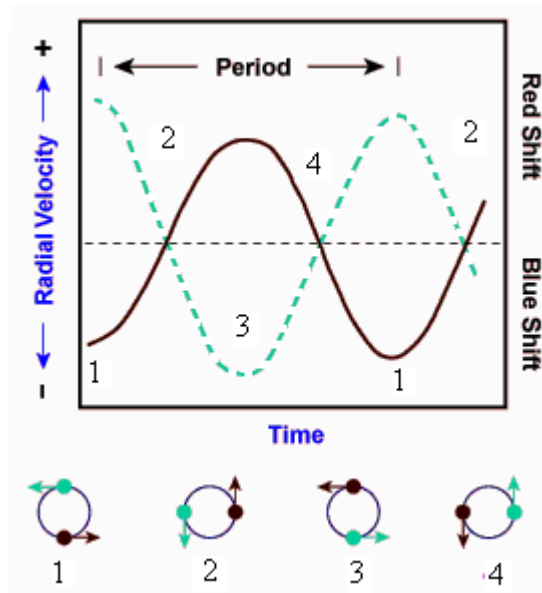


Fig. 3.5 Explanation of the velocity curve of a double spectroscopic binary system

For binaries, for which both spectra can be obtained, and for circular orbits with period  $t$ , following relationship can be obtained.

$$v_1 = \frac{2\pi d_1}{T} \dots\dots\dots(3.5 a)$$

$$v_2 = \frac{2\pi d_2}{T} \dots\dots\dots(3.5 b)$$

Therefore

$$\frac{v_1}{v_2} = \frac{d_1}{d_2} = \frac{M_2}{M_1} \dots\dots\dots (3.6)$$

$v_1$  and  $v_2$  (orbital velocities of the primary and secondary components respectively) can be measured at maximum angular distance of the two stars, because this is the time when radial velocity is equal to actual orbital velocity. They are the maximum velocities of the velocity curve for primary and secondary components respectively. From this (3.5 b), the sum  $d_1 + d_2$  can be determined. With the measured period the sum of the masses can be calculated according to (3.4). From (3.6) the mass ratio can be obtained. With the mass sum and mass ratio, masses of both stars can be determined.

### 3.4 Light curve of eclipsing binaries

The orbital period of the binary system can be measured by plotting a magnitude vs time graph called a light curve. Consider a binary system in which the component stars are both spherical in shape and revolve in circular orbits figure 3.6. **A** is the primary of the system and **B** is the secondary revolving round **A** in a circular orbit. Assuming **B** to start from the extreme left it will be seen to move towards **A** along the line until its disk touches the disk of **A** in position 2. During this period the light received from the system is the total (  $E_1 + E_2$  ) of the full light contribution of **A** ( $E_1$ ) and **B** ( $E_2$ ).

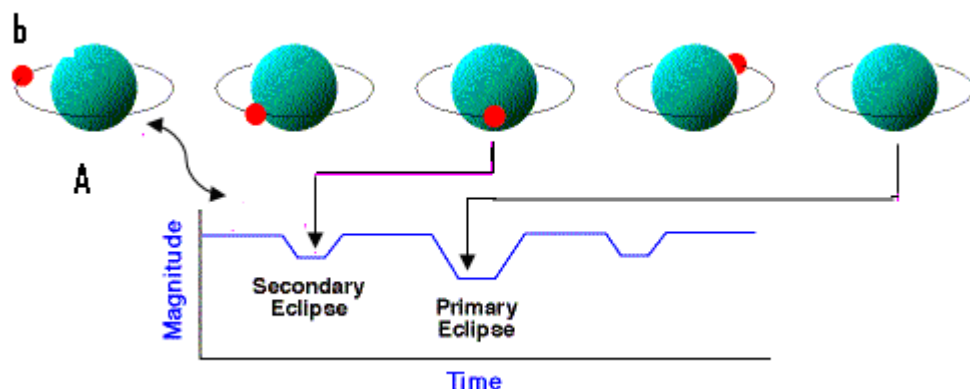


Fig. 3.6 The light curve of an eclipsing binary system

As the disc of B moves in front of A, increasingly larger fractions of the light from A will be intercepted by the disc of B and the light curve will gradually fall down until the whole of disc B is within the disc A in position 3 . At this instant, the light received from the system attains a minimum value and is equal to  $E_2$  plus a fraction of uncovered part of A. As B moves on towards the right the light curve remains steady at the minimum value until disc B touches the rim of disc A. From then onwards disc B will gradually clear out of the disc A and the light from the system will go on increasing until disc B is just out of disc A in position 4 . At this instant the full contribution of A and B are restored. Therefore the light received from the system will remain constant at the same level ( $E_1 + E_2$ ) as before the eclipse started. After B has reached the extreme right, i.e. has completed one half of its revolution, it will begin to move back towards the left. In its leftward journey it will move behind A and will itself be eclipsed by the latter, resulting in another minimum which will be exactly of the same form as the first minimum but of a different depth being equal to the light from A alone. As B revolves round A the two minima will recur at equal intervals as in figure 3.6.

The shape of the minima and the intervals separating them of a light curve depend on the relative sizes, brightness and orbits of the two component stars. Also the limb darkening (star brightness is not uniform all over the disc) of a star and changes to the size of the star cause distortions to the shape of the light curve.

## CHAPTER 4

# INSTRUMENTATION

---

Five major instruments were used in this project.

- 1) Reflective telescope
- 2) Spectrograph
- 3) Charged Coupled Device (CCD) camera
- 4) 12" Schmidt Cassagrain Telescope
- 5) Photoelectric Photometer

### 4.1 GOTO 45cm Cassegrain Telescope



Fig. 4.1 GOTO 45cm Cassegrain Telescope

The GOTO 45 cm Cassegrain Telescope housed at ACCIMT was used to obtain the spectra of the binary system S Ant. The 45 cm Cassagrain Telescope consists of a primary mirror (a parabolic surface with an effective aperture of 450 mm and a focal length of 1800 mm) and a secondary mirror (a hyperbolic surface with an effective aperture of 150 mm. The effective focal length of the telescope is 5400 mm). The f-number of the telescope is 12. The theoretical limiting magnitude of the telescope is 15. This telescope has a German equatorial mount. It is fully computer controlled but also provides the manual controlling functionality. The main telescope has a sub telescope which is aligned parallel with the main telescope. When pointing the main telescope manually to a celestial object we can use the sub telescope as it has a large field of view.

GOTO telescope is equipped with a spectrograph and a photometer which are used to acquire scientific data on celestial objects.

## 4.2 Spectrograph



Fig. 4.2 Monk-Gillieson type Spectrograph

The Monk-Gillieson type Spectrograph is designed to use with the GOTO 45cm telescope. The spectra can be imaged using the SBIG ST-7 CCD camera. The spectrograph and camera body are coupled and mounted as a unit onto the telescope. The theoretical resolving power of this spectrograph  $\lambda/\Delta\lambda$  ( $= mN = 1*1200*64$ ) is 76800. Reflective type plane diffraction gratings with 150, 900 and 1200 grooves/mm can be used on the spectrograph. For our work we used the grating with 1200 grooves/mm to get the 0.29 A/pixel resolution at the wavelength of 6563A.

**Optical Design:** The wide field viewer facilitates identifying the object of interest on the spectrograph. There is also a slit viewer to make sure that the image focuses onto the slit properly. Light enters the spectrograph through an entrance slit and then collimated (made parallel) by the collimation lens. The light impinges upon a reflective diffraction grating, which causes different colors to be reflected at different angles. The light diffracted from the grating is then collected by a focuser, and imaged onto the CCD. This spectrograph has a rectangular slit and the width of the slit should be narrow enough to produce a cylindrical wave front onto the diffraction grating. The width and the height of the slit can be adjusted by turning the two knobs provided on spectrograph. Light of discrete wavelengths through the slit will be imaged on the CCD as vertical lines. If the light does not fill the slit (such as is the case with a faint star) the discrete wavelength will produce a star like point on the CCD, with different wavelengths spread out along a line.

## 4.3 The SBIG ST 7 CCD Camera

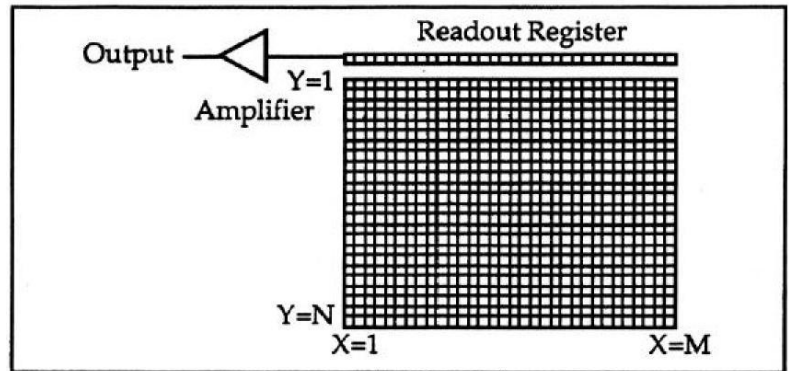


Fig 4.3 (a) ST-7 CCD camera

Fig 4.3 (b) CCD structure

### 4.3.1 Function of the CCD camera

The highly sensitive detectors amplify the tiny currents, which are generated by photons coming from faint objects. The light sensing area of the CCD is only 2.5 millimeters on a side, but it contains 32,680 light sensitive photo sites. Each photo site consists of silicon substrata overlaid with an insulating layer of silicon dioxide and a strip of polysilicon above it. Within each line, the photo sites are separated by channel stops, a thin strip of silicon that has Boron atoms implanted. The channel stops block the movement of electrons across columns within the silicon.

When light falls on the CCD, photons pass through the polysilicon and silicon dioxide layer into the silicon. There they interact with atoms in the silicon crystal lattice, knocking electrons off the atoms according to the photoelectric effect. The number of electrons knocked free is proportional to the number of oncoming photons. In a good CCD, about 60% of the incoming photons will knock out an electron. The electrons are trapped in potential well, which are regions in the silicon layer where the electric potential is highest. Each photo site is a potential well. In electronic terminology, the swarm of electrons becomes a “charge packet” trapped in a potential well.

To read out the chip, the serial register is cleared and the imaging area is cycled once delivering one line’s worth of charge packets to the serial register (fig. 4.3b). The line charge is then transferred to an amplifier. Once again the image area is cycled and the next line’s worth of charge packets enters the serial register. The process is repeated until every charge packet of every line is delivered to the amplifier.

### 4.3.2 Quantum efficiency of the CCD

This is defined as the ratio of the number of photons detected by the camera to the number incident. That is the CCD doesn’t work with the same efficiency in every wavelength. The variation of quantum efficiency with wavelength is shown by the graph provided.

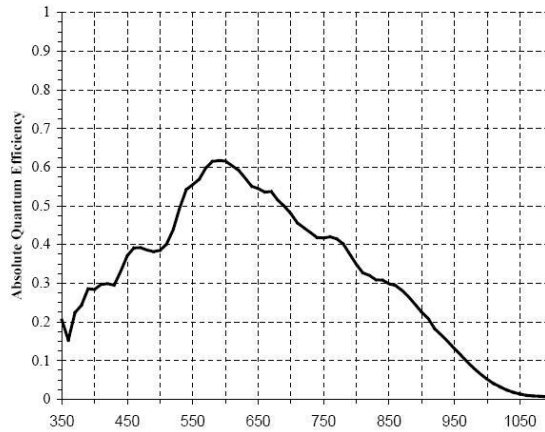


Fig. 4.4 Quantum Efficiency Curve of the SBIG ST 7CCD

### 4.3.3 Dark current

The accumulated charge from thermally generated electrons grows with time. The noise due to dark current is the square root of the number of electrons accumulated during the integration time. Cooling the CCD reduces the rate of generation of thermal electrons.

### 3.3.4 Readout noise

This is the bottom line for noises in the CCD chip, which is due to random variation of the output of the CCD when no signal electrons are present. It is customarily expressed as the root mean square variation in number of electrons detected by the CCD.

### 3.3.5 CCD cooling.

Random readout noise and noise due to dark current combine to place a lower limit on the ability of the CCD to detect faint light sources. By cooling the CCD, the dark current is reduced, allowing long exposures. In fact, for roughly 5 °C of additional cooling, the dark current is reduced by half.

## 4.4 MEADE 12" Schmidt Cassagrain portable Telescope

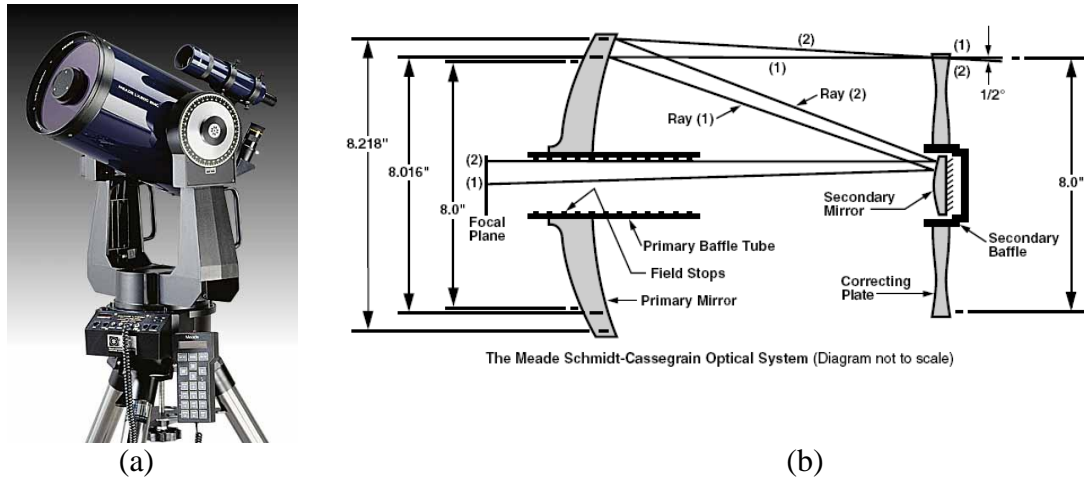


Fig. 4.5 (a) 12" Meade Cassagrain Telescope and (b) The optical system

This Schmidt-Cassegrain 12" telescope has an effective focal length of 3048mm and the f-number of 10. In this telescope model light enters from the right, passes through a thin lens with 2-sided aspheric correction ("correcting plate"), proceeds to a spherical primary mirror, and then to a convex aspheric secondary mirror. The convex secondary mirror multiplies the effective focal length of the primary mirror and results in a focus at the focal plane, with light passing through a central perforation in the primary mirror.

## 4.5 Photoelectric Photometer

For this work we used the OPTEC SSP-5 photometer on the Meade 12" LX 200 portable telescope to obtain photometric data. In this photometer light enters the photometer through the 1/4-inch telescope adapter and is directed either to the focusing eyepiece or the photomultiplier tube (PMT) by means of a flip-mirror. The focusing eyepiece consists of a 1-inch focal length Ramsden and illuminated reticle with a precisely scribed ring that defines the aperture field of view. After a star is centered in the ring, the flip-mirror is rotated to allow light to pass through the aperture stop which separates the star from the background. A Fabry lens then projects an image of the primary mirror/lens onto the photocathode of the PMT.

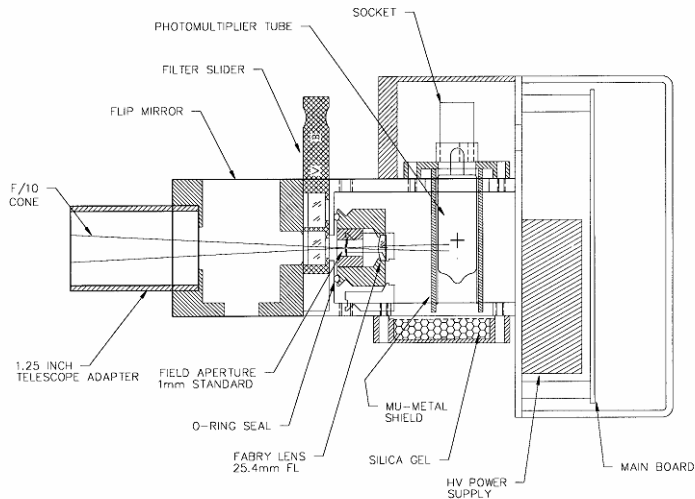


Fig. 4.6 (a) Schematic Optec SSP-5 Photometer

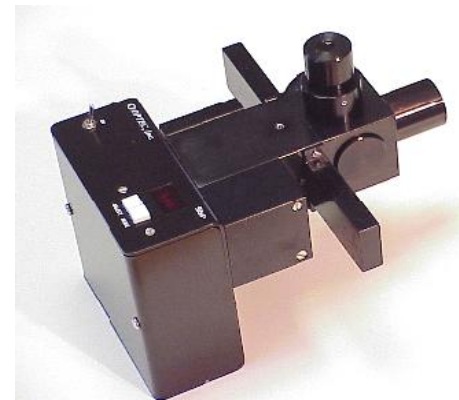


Fig. 4.6 (b) Optec SSP-5

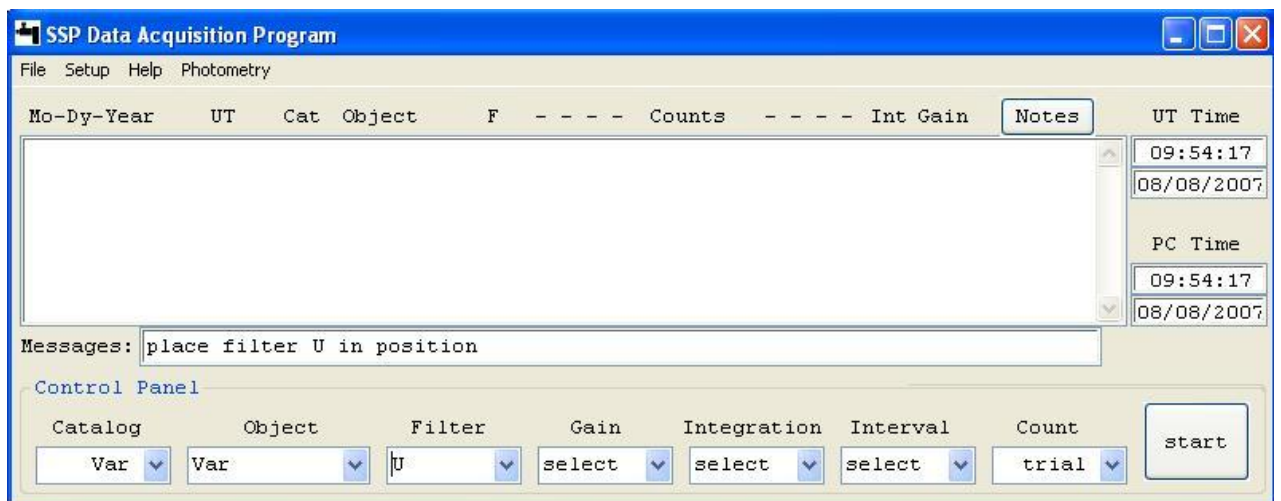


Fig. 4.6c Optec SSP-5 Photometer interface

## CHAPTER 5

# **EXPERIMENTAL PROCEDURE**

---

### **5.1 Obtaining high resolution spectra of S Ant**

Spectroscopic observations were performed on seven days during the period January to May 2007 with the GOTO 45 cm Cassagrain reflective telescope, Monk-Gillieson type Spectrograph and the SBIG ST7 CCD Camera. The diffraction grating with a dispersion axis of 1200 grooves/mm was used. A total of 60 spectra were obtained for S Ant together with spectrum of HD105452 to be used as the radial velocity reference star. The reference star usually is a stable star of the same spectral class as the variable star. The reference star can be used to detect and remove the atmospheric absorptions and emissions (Telluric lines) visible on the spectra.

First and foremost a suitable star, S Ant was found using the General Catalog of Variable Stars (GCVS). The important factors in selecting the binary star were the visibility of the star during the period of observation, the brightness of the star and its period. The Simbad Astronomical data base was used to obtain the characteristics of S Ant (HD 82610). Celestial coordinates and the visual magnitude found from the Simbad data base was used to find the “star number” in the GOTO telescope database. This star number was fed to the telescope operating software. The telescope then compares this information with the data in its star library and points the telescope to the star.

Before acquiring data it had to be verified that the telescope had pointed to the correct star in the sky. This was done using a finding chart, a real image of the sky in the vicinity of the object of interest. The astronomical software called “The Real Sky”, images of real sky survey created by Plomar astronomical observatory was used to get this finding chart of S Ant. The image displayed the actual objects present in the night sky along with the binary system, S Ant. By comparing the stars seen in the wide field viewer of the spectrograph with that of the finding chart, the positioning was verified.

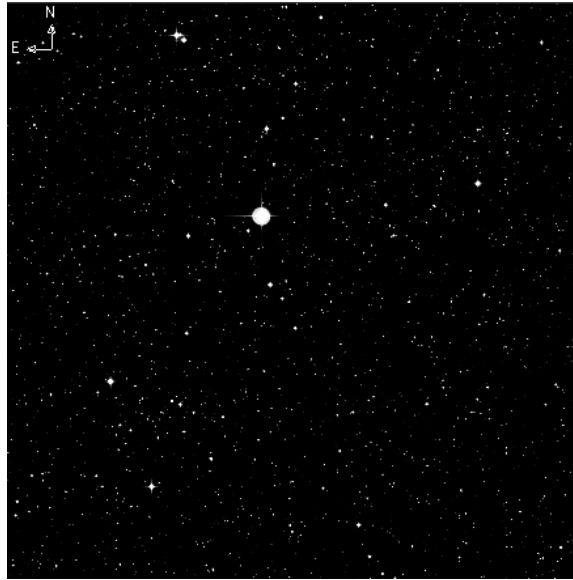


Fig. 5.1 Image of S Ant and its neighboring stars obtained using Real Sky software

The hand set of the telescope was used to make adjustments so that the star was centered on the slit. The next step was to adjust the Fe-Ne hollow cathode lamp current to a sufficient value so that the intensity of the comparison lines is comparable with that of object's spectral lines. In order to reduce the dark currents, the temperature of the CCD chip was set to a low value, around  $-5^{\circ}\text{C}$ .

In order to get a sufficient signal of the stellar spectrum the CCD camera should be exposed long enough. It was a known fact that a 10 minutes exposure for S Ant would suffice. During the exposure of the star the comparison lamp was switched on for about a minute to get its signature on either sides of the stellar spectrum. The CCDOPS software was used to download the spectra onto the computer.

The dark frame with the same exposure time as that of the stellar spectrum was obtained to remove the dark currents from the object's frame. When taking the dark frame CCD camera automatically closes its shutter and allows dark currents to accumulate during the specified exposure time. The telescope was next pointed to the reference star HD105452 and its spectra were obtained following the same procedure.

All spectrums were obtained in the \*.ST7 format. CCDOPS software was used to convert the image format to \*.fit, in order to facilitate the image reduction process in IRAF.

## 5.2 Observation Techniques of Photometry

Observations were performed at Hambanthota using the Meade 12" Cassagrain telescope and Photometer. The observation technique used was Differential Photometry.

### 5.2.1 Differential Photometry

There are basically two different modes of Photometry. These are known as all sky Photometry and differential Photometry.

In All sky Photometry, the count rates of the variable star are compared with that of a standard star in a completely different part of the sky. However, this method requires complete cloud free conditions. This is due to the fact that, the method could give erroneous results if clouds existed in front of the variable star and not in front of the standard star, or vice versa.

In Differential Photometry, the count rates of the variable star are compared with that of a standard star (known as the comparison star) which is situated close by. Therefore it can be assumed that the light from both stars traverse the same thickness of atmospheric layers, allowing the atmospheric extinction corrections to be ignored. If thin clouds exist during exposures, the same fractional amount of light would be reduced from both objects. Thus the ratio of fluxes would not be affected.

Several factors were taken into consideration when selecting the comparison star. The distance between the two objects was less than  $1^\circ$ . This enabled both stars to be measured under similar sky conditions. Also the comparison star had to be a non variable star. Most red stars are known to be variables. Thus they were avoided. HD 105403 was selected as the comparison star with the help of "The Sky" software. In Differential Photometry, the position of the telescope has to be changed constantly to gather photometric data of the comparison star, check star and the sky, in addition to the variable star of interest. Pointing the telescope manually is a tedious task. Therefore a program was written in Visual Basic to control pointing the telescope to stars according to our observation sequence.

For each object three counts were obtained, using four filters U, B, V, I, R for each count. Observations were performed repeating the observing sequence as comparison star, check star and the sky. A limited set of Photometric data was obtained, due to the sky and cloud conditions at Hambanthota and Embilipitiya.

## CHAPTER 6

# DATA ANALYSIS AND RESULTS

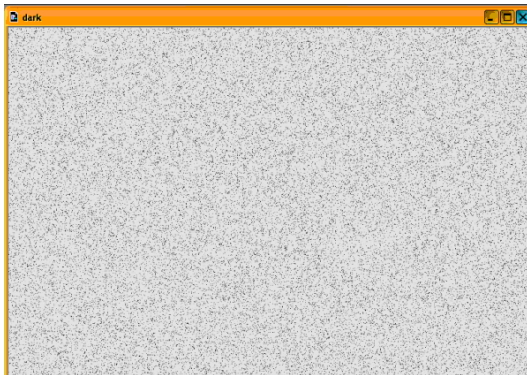
---

### 6.1 Data Reduction and Analysis Procedure

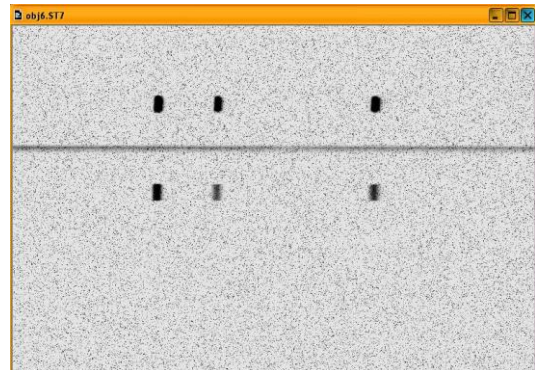
The analysis process for one spectrum is presented in this chapter. CCDOPS which is a Windows based software, and IRAF (Image Reduction and Analysis Facility) which is Linux based software was used for this purpose. The following steps were involved in reducing the data.

#### Dark Subtraction

This was performed using the CCDOPS software. The software allows the image of the star to be displayed. It provides the dark subtraction option where the dark frame is subtracted from the image of the star.



(a) The dark frame



(b) Stellar frame with dark currents



(c) Dark subtracted stellar image

Fig. 6.1 The dark Subtraction (colours inverted)

## Extraction of a 1-D spectrum

The raw spectrum is a 2D (x,y) image. It is convenient to have a 1D spectrum for the spectrum analysis. Therefore a 1D spectrum (Vector) was obtained in IRAF, using the task named “appall”. When the appall task is run, the 2D spectrum is scanned (traced) in the x direction while summing few rows on either side of the center of the spectrum (aperture) to obtain a higher signal. In a 1D spectrum the intensity is available in ADU (Analog to Digital Units) for each pixel in the x direction.



Fig. 6.2 Extracted Stellar image (colours inverted)

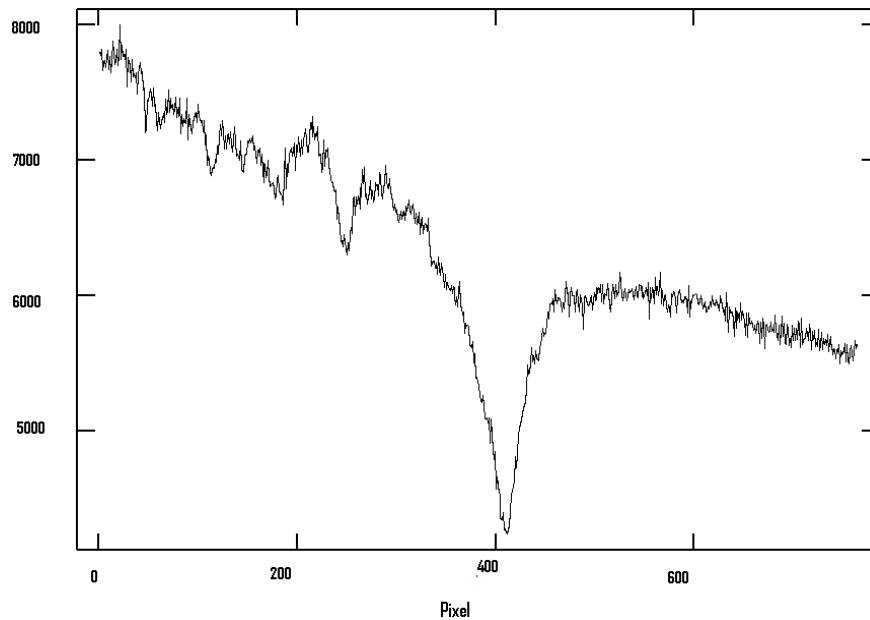


Fig. 6.3 H-  $\alpha$  profile of S Ant (in pixels)

## Wavelength Calibration

For each spectral image of the star, two comparison spectra are formed on top and bottom by the two fiber optic cables which bring light from Fe-Ne discharge lamp. Therefore 1D spectra from both top and bottom comparison spectra were extracted.

However since the comparison spectrum is a discrete spectrum, the image of the star was shifted up, so that the stellar spectrum was brought on top of the comparison spectrum. The package *imshift* and *imarith* was used for this purpose. The comparison spectrum was made continuous by performing these tasks. The *apall* task was then used to trace this comparison spectrum to get a 1D comparison spectrum.

The same procedure was performed to get another 1D spectrum of the comparison lamp by shifting the stellar image to down onto the comparison spectrum

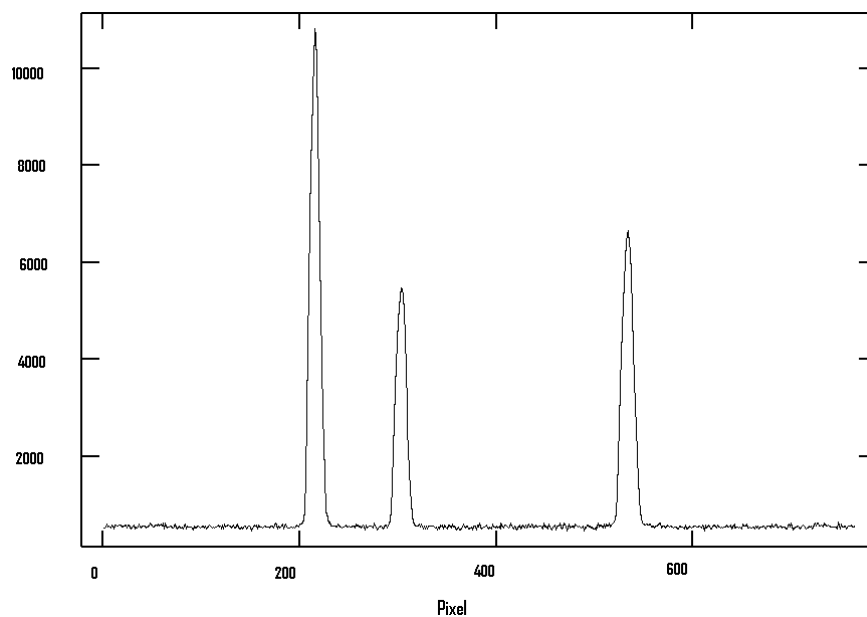


Fig. 6.4 Extracted 1-D spectrum of comparison Fe-Ne Lamp (in pixels)

The Next step was to assign wavelengths to the two comparison spectra. Spectral energy distribution of the emission lines of the comparison spectrum are provided by the manufacturer. The wavelengths are identified by comparing the peak separation and intensities of the extracted spectrum and the Spectral energy distribution given by the manufacturer. The three peaks of the comparison spectrum are assigned the values found using the package *“identify”* of IRAF.

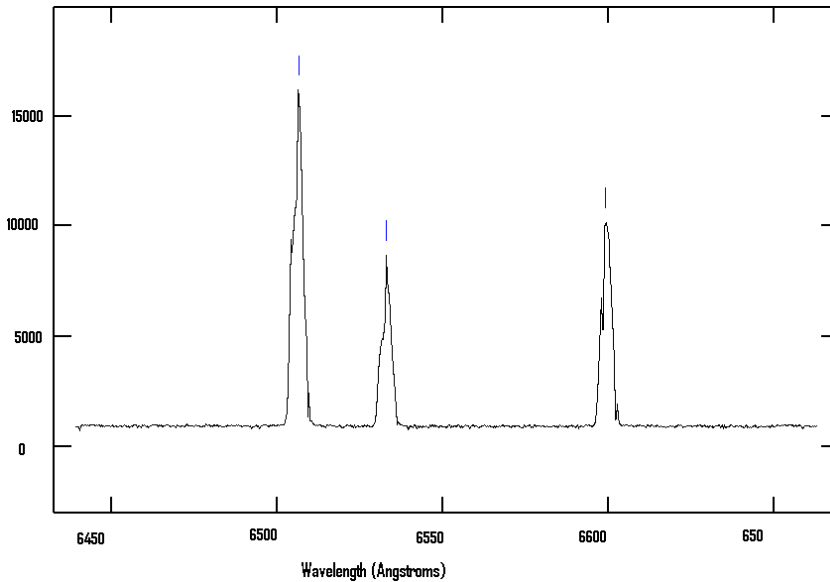


Fig. 6.5 Intensity distribution of reference Fe-Ne spectra (Wavelength in Angstroms)

The pixel values of the extracted 1D spectrum of the star was assigned wavelength values by referring to the two calibrated spectrums of the lamp, using the package “refspectra”. Finally this wavelength solution was applied to the stellar 1D spectrum by running “dispcor” and the image was named by the template \*cal.imh

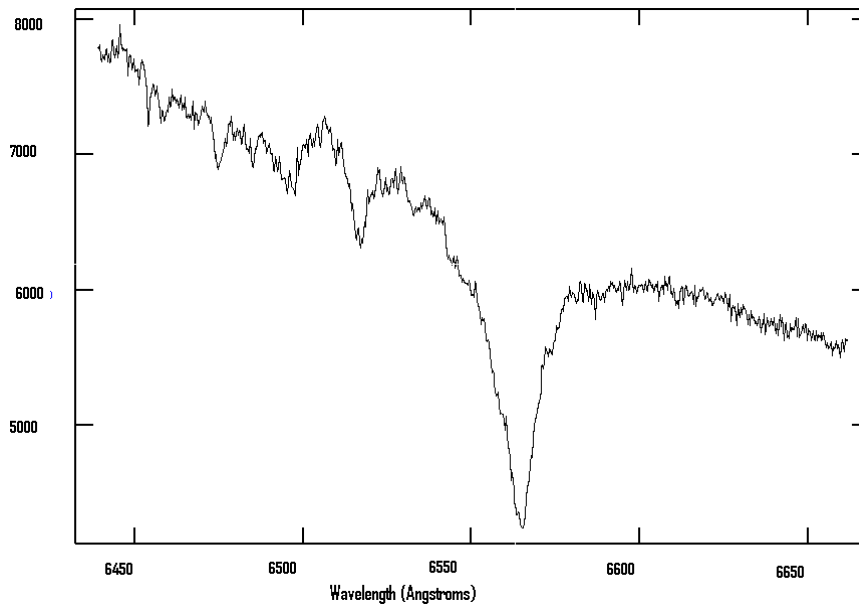


Fig. 6.6 H-  $\alpha$  profile of SAnt (in angstroms)

### Atmospheric correction

This was performed in order to remove the absorption lines present on the spectrum of the star due to water vapor and gases present in the earth’s atmosphere. The spectrum of the star was “divided” by the of the standard reference star. The IRAF task “sarith” was used to perform this dividing of spectra.

## Normalization to a stellar continuum

This was performed to bring the intensities of the entire continuum to unity. This is particularly important for the intensity comparisons of several spectra.

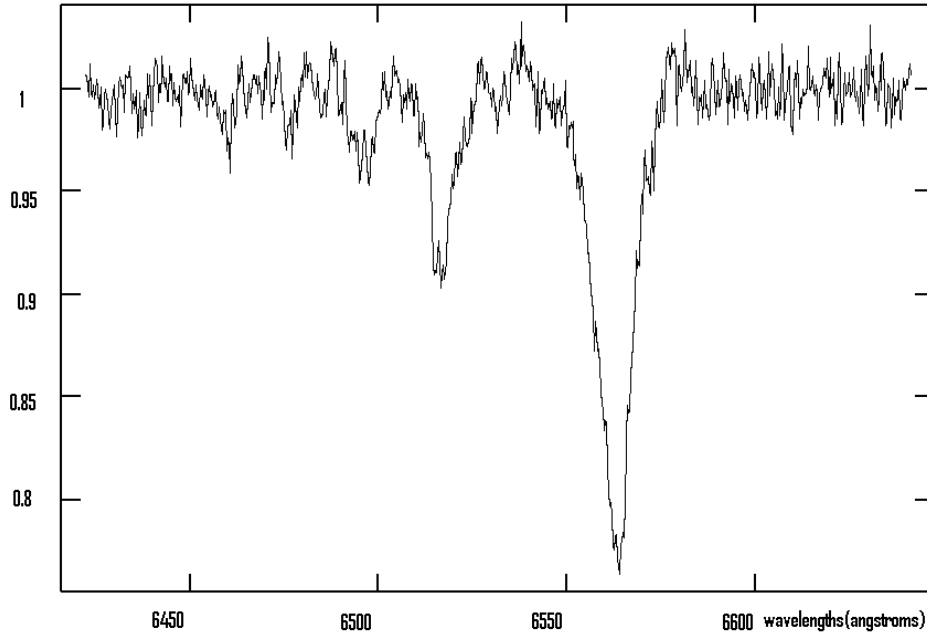


Fig. 6.7 The normalized spectrum

## Radial Velocity calculation

The calibrated spectrum was displayed on the spectrum viewer on IRAF called “splot” which runs on the graphical terminal named “irafterm”. Splot displays a graph of flux versus wavelength of the spectrum. The spectrum was smoothed by running boxcar average method of box size 3.

The reference velocity point on the H alpha line profiles is the laboratory frame wavelength of the H alpha absorption line (6562.8 Å). The wavelength scale of the stellar spectrum was then converted to the velocity scale by using the “v” option given in *splot*.

In order to find the velocity curve of S Ant we should find the shift in the velocity of the H alpha absorption line with the phase. As S Ant is a double line spectroscopic binary we get H alpha line profiles of both components. These two H alpha profiles are blended and their fluxes are different. It is very difficult to find the center of the H alpha profile of the fainter component as it is blended with the brighter component. To find the centers of these two H alpha line profiles the “Gaussian Profile Fit” method and “Deblending method” were used.

In the former method two centers of the profiles were obtained by visually observing and manually fitting two Gaussian profiles at the points where the peaks appear. The latter case works in such a way that the deblending of the two profiles is done by fitting the Gaussian (Lorentzian or Voigt profile types can also be selected) profiles to the deblended line profile by taking into account the marked line profile centers.

## Gaussian Fit Method

In order to find the center of a spectral line, the option of fitting a Gaussian profile on Splot was used. A Gaussian profile for the peak shifted towards the left side (from reference point) was fitted using the keys *h* and *l*. Keys *h* and *r* were used to fit the Gaussian profile with center shifted towards the right side. Using this method the velocities of the line profiles of the two components of S Ant were calculated.

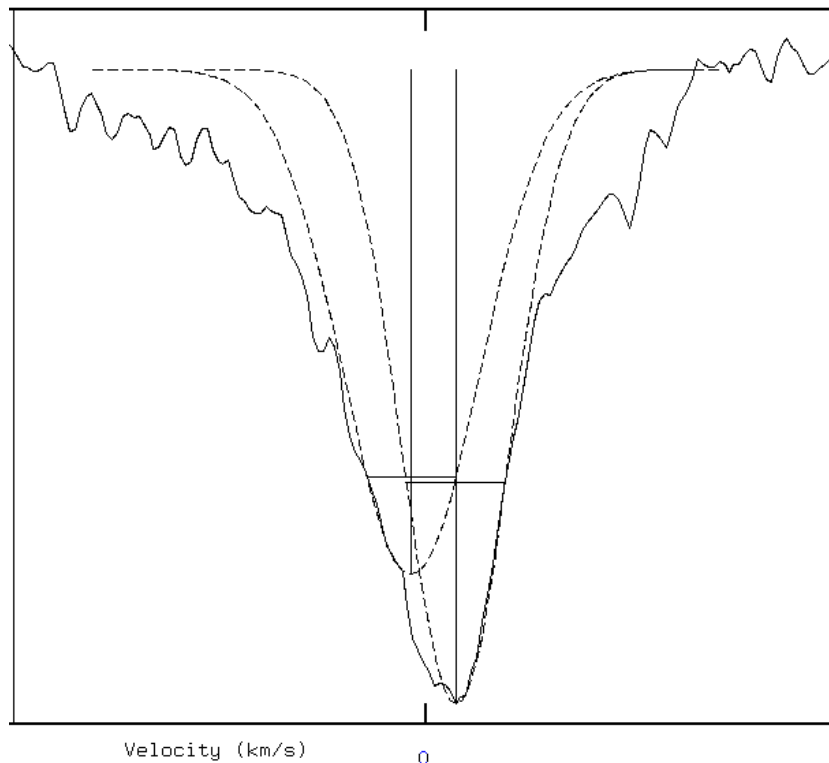


Fig. 6.8 Two Gaussian profiles fit to the peaks of the spectrum

## Deblending Method

In this method the either sides of the continuum of blended line profile was marked by using the option key “d” given in the splot. Two centers of the bended lines were roughly estimated and marked on the spectrum. Splot then fits the blended profile with two Gaussian profiles (a Gaussian fit was selected for this analysis) by considering the marked approximated profile centers. Calculated deblended profile centers, corresponding to the two components of the binary system were obtained in this manner for each spectrum.

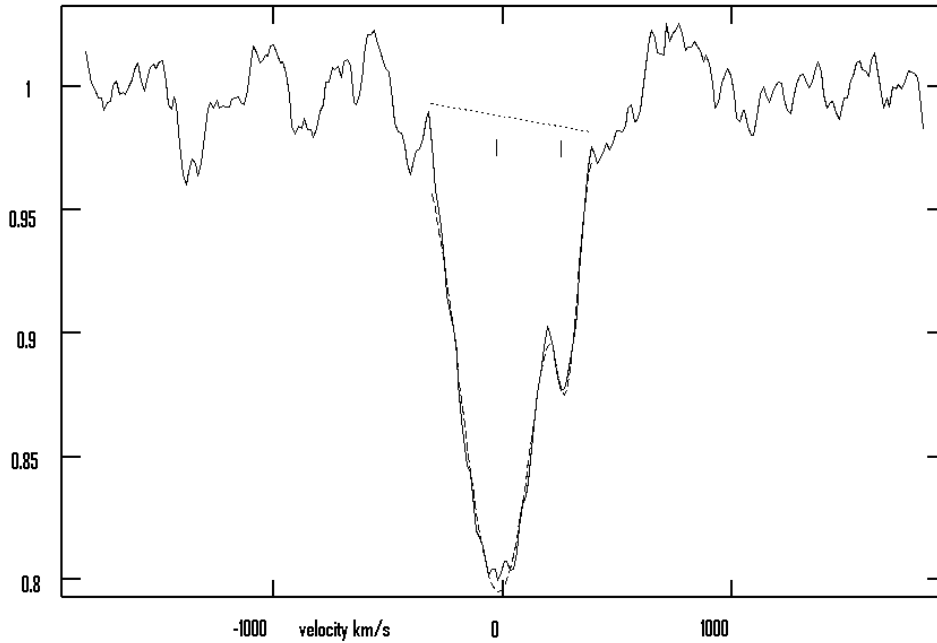


Fig 6.9 The debrending method

## Broadening Function method

This was used as a third method for calculating the radial velocities. The underlying theory in this method is a linear deconvolution. Supposing the convolution operation maps a sharp lined spectrum  $T$  through another function  $B$ , into a broadened spectrum of a binary star,  $B(\lambda)$  known as the broadening function, can be calculated taking Fourier transform and its inverse transform as shown below.

$$P(\lambda') = B(\lambda) * T(\lambda) = \int B(\lambda' - \lambda)T(\lambda)d\lambda$$

$$F\{P(\lambda')\} = F\{B(\lambda)\}.F\{T(\lambda)\}$$

$$B(\lambda) = F^{-1}\{F\{P(\lambda')\}/F\{T(\lambda)\}\}$$

The broadening function  $B$  in fact corresponds to the spectrum with debrended peaks. A windows based version of the original IDL software (created by Rucinski) was used for this purpose. The calibrated *.imh* files were converted back to the fits form and were fed to the software along with a sharp lined reference spectrum. The peak positions were obtained and velocity values were calculated.

## Radial velocity correction

The radial velocity of the binary star observed from the earth should be corrected for the rotation of the earth, the motion of the earth about the earth-moon barycenter and the orbit of the barycenter about the sun. This corrected velocity is called the heliocentric velocity which is measured with respect to Sun. IRAF contains a package *rvcorrect* which facilitates this calculation when the date and time of the observed spectrum, observatory location and the observed radial velocity are provided, so that the output is directly added or subtracted from the radial velocity, which was calculated previously.

## 6.2 Results

### 6.2.1 Gaussian Profile Fit method

Table 6.1 Velocity calculations for the Primary star using the H-alpha line

Phase	Observed Velocity (km/s))	Heliocentric Correction (km/s)	Heliocentric Velocity (km/s)
0.08828	14.59733	2.99	17.58733
0.11556	52.0561	2.95	55.0061
0.13137	47.59113	2.93	50.52113
0.17399	70.9948	2.86	73.8548
0.18764	56.40505	2.84	59.24505
0.20275	18.07188	2.82	20.89188
0.27476	-18.4859	7.13	-11.3559
0.28886	8.797896	2.66	11.457896
0.30457	-34.7998	2.63	-32.1698
0.31846	-11.2923	2.61	-8.6823
0.34647	32.84413	2.15	34.99413
0.3536	-20.1776	6.99	-13.1876
0.36191	13.79196	2.12	15.91196
0.47547	-28.9553	10.39	-18.5653
0.54206	27.54295	6.26	33.80295
0.56079	4.031197	6.23	10.261197
0.57861	44.56381	9.83	54.39381
0.58309	46.58556	6.19	52.77556
0.60629	16.19426	13.72	29.91426
0.63643	35.97325	13.66	49.63325
0.64114	72.88185	6.12	79.00185
0.65369	26.7606	13.85	40.6106
0.66844	100.4262	13.6	114.0262
0.7345	47.46332	12.96	60.42332
0.74834	47.46332	12.94	60.40332
0.76181	101.46	12.91	114.37
0.81657	58.80908	12.81	71.61908
0.82161	72.79341	13.35	86.14341
0.83124	60.03044	12.79	72.82044
0.8579	33.97793	12.74	46.71793
0.87441	18.89496	12.72	31.61496
0.88681	40.70152	13.59	54.29152
0.88823	26.24548	12.7	38.95448
0.90188	9.0902	12.68	21.7702
0.91568	20.15107	12.66	32.81107
0.9526	-3.16712	12.61	9.44288

**Table 6.2 Velocity calculations for the Secondary star using the H-alpha line**

Phase	Observed Velocity (km/s)	Heliocentric Correction (km/s)	Heliocentric Velocity (km/s)
0.11556	186.7854	2.95	189.7354
0.13137	207.4511	2.93	210.3811
0.15949	210.0791	2.89	212.9691
0.17399	230.6464	2.86	233.5064
0.20275	220.9426	2.82	223.7626
0.28886	227.0333	2.66	229.6933
0.30457	217.7864	2.63	220.4164
0.36191	162.0679	2.12	164.1879
0.47547	59.34028	10.39	69.73028
0.65369	-158.4809	13.85	-144.6309
0.68302	-204.4848	13.58	-190.9048
0.7345	-165.7489	12.96	-152.7889
0.74358	-187.2776	12.79	-174.4876
0.76181	-131.1623	12.91	-118.2523
0.77427	-163.6368	13.42	-150.2168
0.78129	-131.1456	12.88	-118.2656
0.82161	-92.3764	13.35	-79.0264

## 6.2.2 Deblending Method

**Table 6.3 Velocity calculations for the Primary star using the H-alpha line**

Phase	Observed Velocity (km/s)	Heliocentric Correction (km/s)	Heliocentric Velocity (km/s)
0.11556	37.1057	2.95	40.0557
0.13137	73.1188	2.93	76.0488
0.14408	29.3004	2.91	32.2104
0.15949	69.6544	2.89	72.5444
0.17399	61.3008	2.86	64.1608
0.18764	-1.02093	2.84	1.81907
0.20275	-16.6444	2.82	-13.8244
0.27476	-25.993	7.13	-18.863
0.28886	-41.6386	2.66	-38.9786
0.30457	-52.1192	2.63	-49.4892
0.31846	-30.8922	2.61	-28.2822
0.34647	-20.6479	2.15	-18.4979
0.3536	-51.1725	6.99	-44.1825
0.36191	-57.3178	2.12	-55.1978
0.65369	62.881	13.85	76.731
0.66844	60.3095	13.6	73.9095
0.7345	71.0108	12.96	83.9708
0.74834	70.4246	12.94	83.3646
0.75928	80.907	13.86	94.767
0.76181	81.7782	12.91	94.6882
0.81657	67.6466	12.81	80.4566
0.82161	79.1371	13.35	92.4871
0.83124	62.476	12.99	75.466

**Table 6.4 Velocity calculations for the Secondary star using the H-alpha line**

Phase	Observed Velocity (km/s)	Heliocentric Correction (km/s)	Heliocentric Velocity (km/s)
0.11556	148.297	2.95	151.247
0.13137	171.975	2.93	174.905
0.14408	139.165	2.91	142.075
0.15949	171.976	2.89	174.866
0.17399	187.323	2.86	190.183
0.18764	216.09	2.84	218.93
0.20275	209.043	2.82	211.863
0.28886	240.545	2.66	243.205
0.30457	233.096	2.63	235.726
0.31846	267.953	2.61	270.563
0.34647	219.667	2.15	221.817
0.3536	152.497	6.99	159.487
0.36191	154.857	2.12	156.977
0.64781	-98.6494	13.12	-85.5294
0.65369	-185.416	13.85	-171.566
0.66844	-168.555	13.6	-154.955
0.7345	-183.694	12.96	-170.734
0.74358	-190.399	12.79	-177.609
0.74834	-197.278	12.94	-184.338
0.76181	-236.961	12.91	-224.051
0.77427	-135.573	13.42	-122.153
0.78129	-152.21	12.88	-139.33
0.80663	-102.955	13.37	-89.585
0.82161	-85.8162	13.35	-72.4662
0.83124	-83.5951	12.79	-70.8051

### 6.2.3 Broadening Function method

**Table 6.5 Velocity calculations for the Primary and secondary stars using the H-alpha line**

Phase	Radial Velocity (km/s)			Heliocentric velocity km/s
	Primary	Secondary	Correction km/s	Primary
0.11556	30.971	Not available	2.95	33.921
0.17399	46.318	268.55	2.86	49.178
0.18764	41.762	288.37	2.84	44.602
0.20275	25.676	246.35	2.82	28.496
0.21846	28.661	267.19	2.75	31.411
0.27476	10.823	243.54	7.13	17.953
0.28886	7.9389	273.14	2.66	10.5989
0.31846	11.476	268.63	2.61	14.086
0.34647	20.222	286.47	2.15	22.372
0.3536	12.608	265.04	6.99	19.598
0.36191	-7.9196	258.42	2.12	-5.7996
0.54206	27.694	Not available	6.26	33.954
0.56079	39.071	Not available	6.23	45.301

0.58309	44.931	Not available	6.19	51.121
0.6063	19.26	Not available	13.72	32.98
0.63644	-19.961	Not available	13.66	-6.301
0.64781	41.182	Not available	13.12	54.302
0.66844	67.742	Not available	13.6	81.342
0.68303	74.825	Not available	13.58	88.405
0.70388	21.27	-267.3	13.54	34.81
0.74359	55.969	-290.08	12.79	68.759
0.74834	49.874	-259.27	12.94	62.814
0.75928	92.457	-256.16	12.96	105.417
0.76182	58.176	-265.77	12.91	71.086
0.77427	29.234	Not available	13.42	42.654
0.7813	45.344	-249.04	12.88	58.224
0.79059	26.637	-224.55	13.39	40.027
0.80664	73.856	Not available	13.37	87.226
0.81657	66.404	Not available	13.35	79.754
0.82162	46.416	-242.94	13.35	59.766
0.83125	29.409	-249.76	12.79	42.199
0.84466	8.8869	-253.75	12.77	21.6569
0.8579	33.071	-244.42	12.74	45.811
0.88823	30.933	-206.45	12.7	43.633
0.91569	14.541	Not available	12.66	27.201
0.95261	22.548	Not available	12.61	35.158

**Table 6.6 Velocity calculations for the Primary star using Fe (5285.85 A, 5167.49 A) and Al (5171.6 A) lines**

Phase	Observed Velocity (km/s)	Heliocentric Correction (km/s)	Heliocentric Velocity (km/s)
0.16654	-37.728	3.947	-33.781
0.19916	-52.443	-22.404	-74.847
0.26027	-67.362	-1.15	-68.512
0.27599	-60.274	-0.372	-60.619
0.29193	-50.549	-3.95	-54.499
0.31200	-41.594	-9.771	-51.356

## 6.3 Radial velocity curves of S Ant

### 6.3.1 Gaussian Fit method

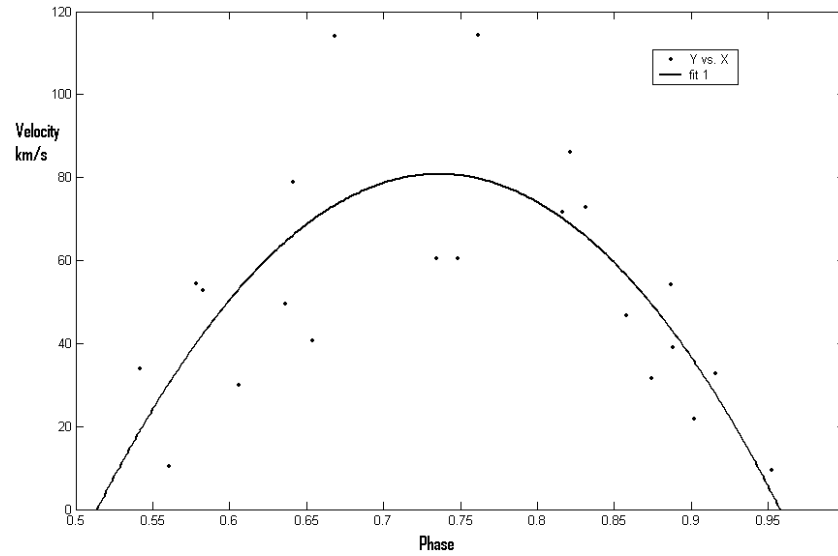


Fig. 6.1 Velocity curve for the Primary component (phase 0.5-1)

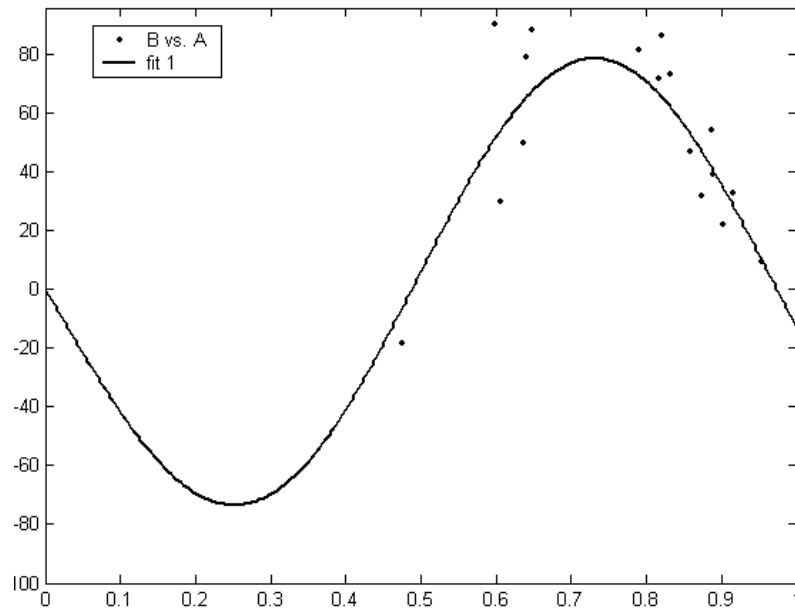


Fig. 6.2 Velocity curve for the Primary component (extrapolated)

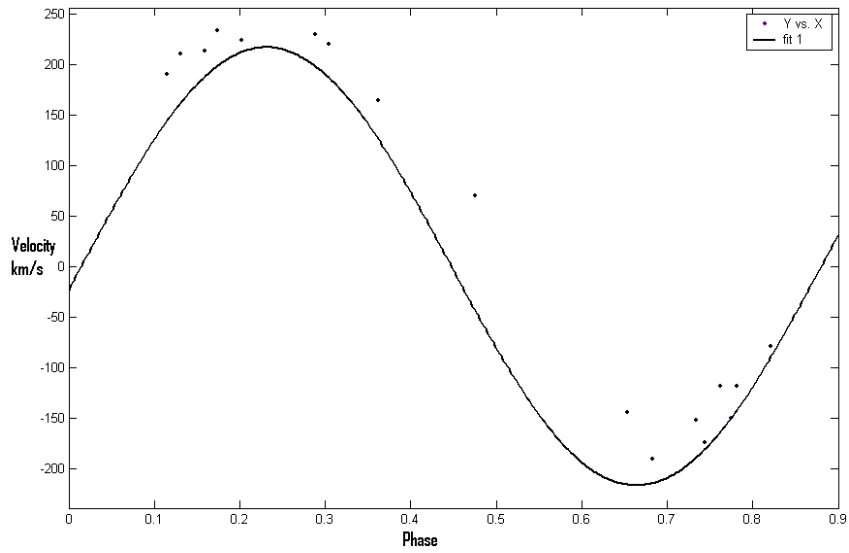


Fig 6.3 Velocity curve of the secondary component

### 6.3.2 Deblending Method

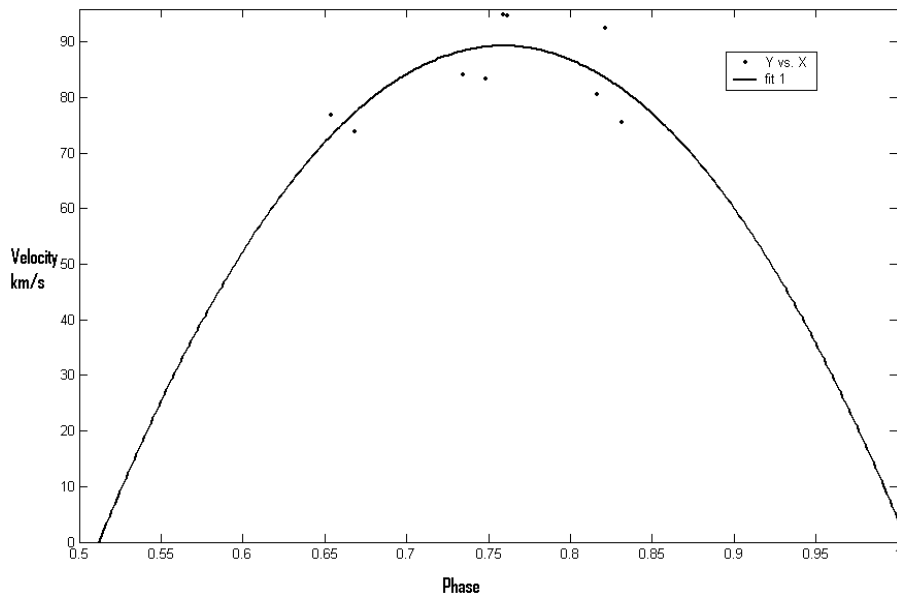


Fig 6.4 Velocity curve of the primary component

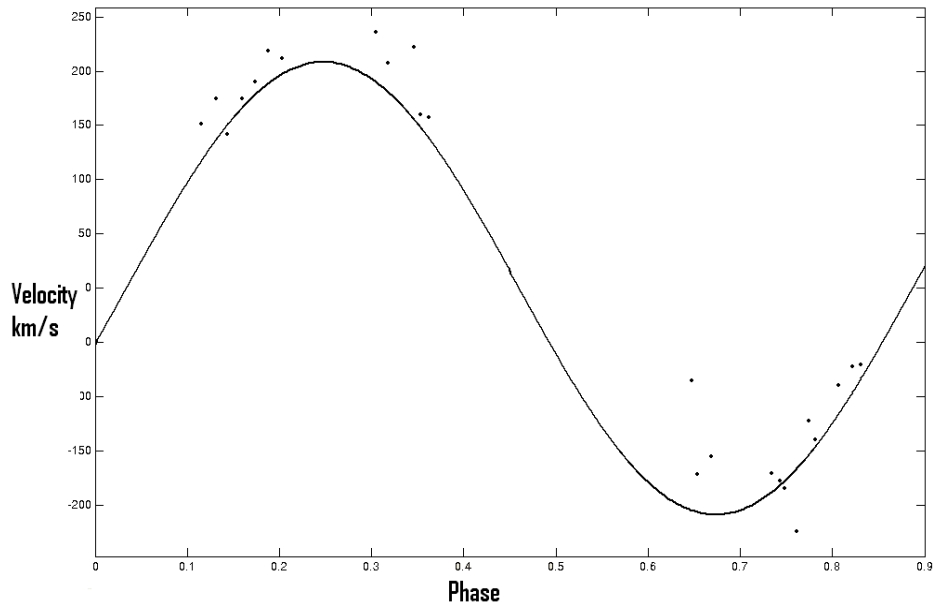


Fig 6.5 Velocity curve of the secondary component

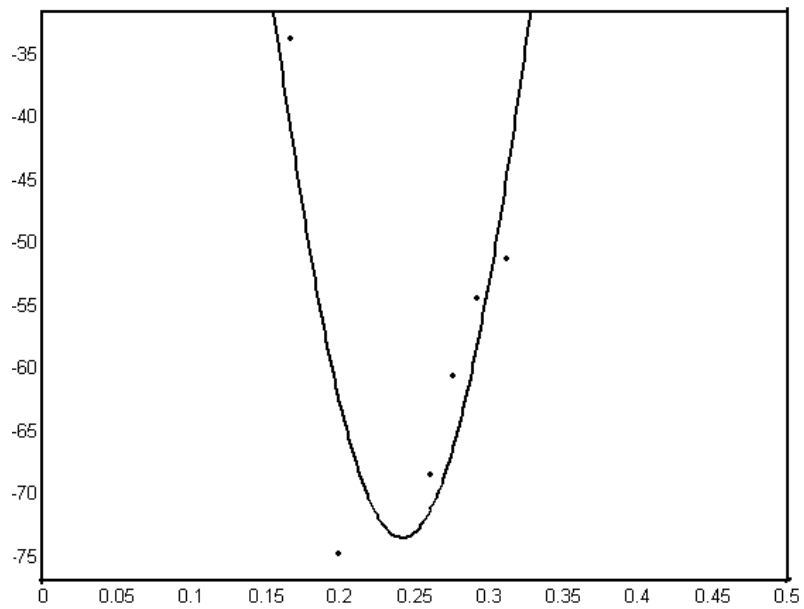


Fig. 6.8 Velocity curve for the Primary star using metallic lines

### 6.3.3 Broadening Function method

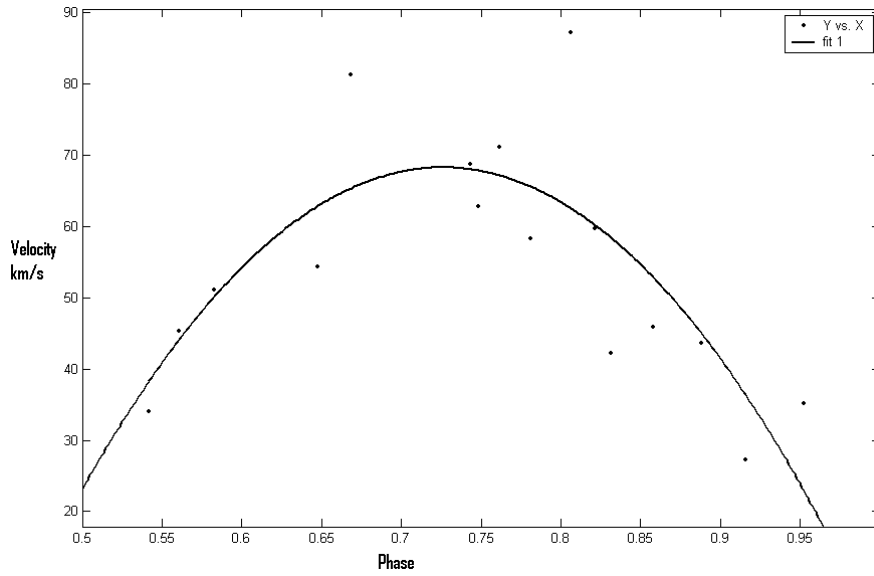


Fig 6.6 Velocity curve of the Primary component

## 6.4 Photometric Data

Table 6.5 Photometric data and light curve measurements

Date	time(local)	Object	Filter	Count1	Count2	Count3	Average Count	Sky Subtract
2/16/2007	3:36:56	COMP	U	170	173	177	173.3333333	12.66666667
2/16/2007	3:37:09	COMP	B	576	562	495	544.3333333	367.6666667
2/16/2007	3:37:28	COMP	V	1859	1572	1763	1731.3333333	1543.6666667
2/16/2007	3:37:45	COMP	R	2109	2340	2195	2214.6666667	2025.3333333
2/16/2007	3:37:59	COMP	I	164	158	159	160.3333333	0
2/16/2007	3:39:15	SKY	U	163	161	158	160.6666667	
2/16/2007	3:39:27	SKY	B	176	176	178	176.6666667	
2/16/2007	3:39:38	SKY	V	188	186	189	187.6666667	
2/16/2007	3:39:55	SKY	R	189	190	189	189.3333333	
2/16/2007	3:40:08	SKY	I	159	161	161	160.3333333	
2/16/2007	3:42:17	VAR	U	234	219	228	227	66.33333333
2/16/2007	3:42:32	VAR	B	1071	956	925	984	807.3333333
2/16/2007	3:42:42	VAR	V	1832	1692	1789	1771	1583.333333
2/16/2007	3:42:53	VAR	R	1765	1584	1657	1668.6666667	1479.333333
2/16/2007	3:43:05	VAR	I	167	160	162	163	2.666666667
2/16/2007	3:47:48	CHECK	U	167	167	170	168	7.333333333
2/16/2007	3:47:58	CHECK	B	247	253	250	250	73.33333333
2/16/2007	3:48:10	CHECK	V	370	359	350	359.6666667	172
2/16/2007	3:48:23	CHECK	R	363	357	375	365	175.6666667
2/16/2007	3:48:35	CHECK	I	159	157	160	158.6666667	-1.666666667
2/16/2007	3:53:57	COMP	U	170	175	172	172.3333333	10.66666667
2/16/2007	3:54:09	COMP	B	497	429	475	467	288.6666667
2/16/2007	3:54:20	COMP	V	616	620	1151	795.6666667	602.3333333
2/16/2007	3:54:39	COMP	R	209	211	201	207	18.33333333
2/16/2007	3:54:49	COMP	I	164	159	153	158.6666667	-1.666666667
2/16/2007	3:55:28	SKY	U	163	166	156	161.6666667	
2/16/2007	3:55:38	SKY	B	178	178	179	178.3333333	
2/16/2007	3:55:50	SKY	V	196	194	190	193.3333333	
2/16/2007	3:56:06	SKY	R	192	189	185	188.6666667	
2/16/2007	3:56:19	SKY	I	158	162	161	160.3333333	
2/16/2007	3:59:36	VAR	U	213	219	221	217.6666667	56
2/16/2007	3:59:45	VAR	B	815	891	833	846.3333333	668
2/16/2007	4:00:07	VAR	V	1411	1287	1150	1282.6666667	1089.333333
2/16/2007	4:00:22	VAR	R	1116	1248	975	1113	924.3333333
2/16/2007	4:00:33	VAR	I	161	162	157	160	-0.333333333
2/16/2007	4:03:26	COMP	U	172	168	172	170.6666667	11.66666667
2/16/2007	4:03:40	COMP	B	394	409	450	417.6666667	244.6666667
2/16/2007	4:03:52	COMP	V	1466	1446	1226	1379.3333333	1185.333333
2/16/2007	4:04:08	COMP	R	2166	2050	1918	2044.6666667	1854.6666667
2/16/2007	4:04:24	COMP	I	159	160	160	159.6666667	2.333333333
2/16/2007	4:14:08	SKY	U	158	156	163	159	
2/16/2007	4:14:29	SKY	B	169	171	179	173	
2/16/2007	4:14:44	SKY	V	194	195	193	194	
2/16/2007	4:14:56	SKY	R	192	191	187	190	
2/16/2007	4:15:08	SKY	I	156	162	154	157.3333333	
2/16/2007	4:18:00	VAR	U	177	172	178	175.6666667	16.66666667

2/16/2007	4:18:14	VAR	B	392	401	415	402.6666667	229.6666667
2/16/2007	4:18:24	VAR	V	827	841	736	801.3333333	607.3333333
2/16/2007	4:18:37	VAR	R	848	784	732	788	598
2/16/2007	4:18:50	VAR	I	161	160	159	160	2.66666667
2/16/2007	4:22:48	COMP	U	164	163	165	164	6.33333333
2/16/2007	4:23:01	COMP	B	231	227	241	233	73.66666667
2/16/2007	4:23:15	COMP	V	490	445	495	476.6666667	318
2/16/2007	4:23:47	COMP	R	303	256	221	260	99
2/16/2007	4:23:59	COMP	I	160	160	155	158.3333333	-1.66666667
2/16/2007	4:25:57	SKY	U	160	158	155	157.6666667	
2/16/2007	4:26:07	SKY	B	159	162	157	159.3333333	
2/16/2007	4:26:19	SKY	V	161	156	159	158.6666667	
2/16/2007	4:26:31	SKY	R	162	157	164	161	
2/16/2007	4:26:41	SKY	I	159	162	159	160	
2/16/2007	4:29:06	VAR	U	164	168	164	165.3333333	7.66666667
2/16/2007	4:29:17	VAR	B	277	279	265	273.6666667	114.3333333
2/16/2007	4:29:28	VAR	V	460	459	442	453.6666667	295
2/16/2007	4:29:38	VAR	R	594	595	481	556.6666667	395.6666667
2/16/2007	4:29:47	VAR	I	157	159	159	158.3333333	-1.66666667
2/16/2007	4:32:08	COMP	U	162	161	165	162.6666667	5
2/16/2007	4:32:19	COMP	B	202	224	221	215.6666667	56.33333333
2/16/2007	4:32:31	COMP	V	441	419	424	428	269.3333333
2/16/2007	4:32:46	COMP	R	505	552	560	539	378
2/16/2007	4:32:56	COMP	I	160	157	162	159.6666667	-0.33333333

phase	$\Delta u$	phase	$\Delta b$	phase	$\Delta v$	Phase	$\Delta R$
-	-	-	-	-	-	-	-
0.154363	1.79767	0.154537	-0.854	3:42	-0.02755	0.15478	0.341076
0.166389	-1.8004	0.166493	-0.91095	4:00	0.726033	0.166921	-4.25647
-	-	-	-	-	-	-	-
0.179167	0.38725	0.179329	0.068692	4:18	0.430098	0.179595	1.228912
-	-	-	-	-	-	-	-
0.186875	0.20744	0.187002	-0.47725	4:29	1.54987	0.187245	-1.50424

## 6.5 Calculations

Primary Component	Gaussian Profile Fit		Deblending Method	
	Phase	Peak velocity km/s	Phase	Peak velocity km/s
	0.73621	80.8687	0.75896	89.261
Secondary Component	0.23061	216.864	0.24742	208.59
	0.66420	-216.865	0.67374	-208.589

Using the results of the deblending method and averaging the magnitudes of the two peak velocities where appropriate it can be estimated that,

$$v_1 = 89.261 \text{ Km/s} \quad v_2 = 208.589 \text{ Km/s}$$

Where  $v_1$  and  $v_2$  are the orbital velocities of the primary and secondary components respectively.

Equation 3.6 gives

$$\frac{v_1}{v_2} = \frac{d_1}{d_2} = \frac{M_2}{M_1}$$

$$\frac{M_2}{M_1} = \frac{v_1}{v_2}$$

The peaks of the velocity curve correspond to the orbital velocities of the two components of the binary system

$$v_1 = 89.261 \text{ Km/s} \quad v_2 = 208.589 \text{ Km/s}$$

$$\frac{M_2}{M_1} = \frac{89.261}{208.589} = 0.42$$

$$M_1 + M_2 = \frac{4 \pi^2 (d_1 + d_2)^3}{T^2 G} \dots\dots\dots 3.4$$

from equations 3.5 a and 3.5 b

$$d_1 + d_2 = \frac{T}{2\pi} (v_1 + v_2) \text{ and substituting this in 3.4,}$$

$$M_1 + M_2 = \frac{(v_1 + v_2)^3}{2\pi G} T$$

Using T= 0.6484d, obtained from a previous study and substituting for G, v<sub>1</sub> and v<sub>2</sub>

$$M_1 + M_2 = \frac{[(89.261+208.589) \times 10^3 \text{ms}^{-1}]^3}{2\pi \times 6.67 \times 10^{-11} \text{m}^3 \text{s}^{-2} \text{kg}^{-1}} \times 0.6484 \times 24 \times 3600 \text{s}$$

$$M_1 + M_2 = 3.532 \times 10^{30} \text{ kg}$$

using

$$M_2 = 0.42M_1$$

$$M_1 = 2.487 \times 10^{30} \text{ kg}$$

$$M_2 = 1.045 \times 10^{30} \text{ kg}$$

## CHAPTER 7

# DISCUSSION AND CONCLUSION

The Prime objective of this study is to calculate the spectroscopic mass ratio of the binary system S Ant. Spectroscopic data alone is sufficient for this calculation. Therefore this study focuses mainly on Spectroscopy. However, other parameters such as individual masses of the two components can be obtained provided that the period of the binary system is known.

It must be mentioned here that the purpose of photometry is to find out the period of the system, through which any changes of the period can be determined. This is particularly significant since the period of contact binaries tend to change with time when mass transfer from one component to other occurs. In order to calculate additional parameters of the binary system we can adopt the period of the binary system from the latest available photometric studies done on this system. The period  $P = 0.6484$  days of the system was adopted Slavek M Rucinski (1997).

**Limitations:** Performing photometry was extremely difficult because of the poor sky conditions during the period of observation. Several attempts made to obtain the Photometric data at different parts of the country such as Hambanthota, Embilipitiya and Katubedda failed due to the cloudy sky conditions. Also the few obtained photometric data seem to be scattered and unrealistic because of the appearance of clouds during the time when the data was gathered.

Another great limitation that came across when conducting this study was the light gathering power of the telescope. It is observed that to obtain spectra with high signal to noise ratio the spectra of S Ant should be exposed more than 20 minutes. This is also not possible because the period of the S Ant is small and the spectral lines smear if the spectrum is exposed for long.

**Difficulties faced:** In all the spectra that were obtained in this study, only the H alpha absorption line of the primary component is explicitly visible. We have noticed the H alpha absorption line of the secondary component blended with the primary component. One reason for this could be because S Ant is a contact binary and its absorption lines are broad and blended. Therefore several methods were adopted to find the center of the blended weak component. It must be mentioned here that this part of the project required additional effort since blending of peaks was totally unexpected.

When calculating the velocities using the first method (Gaussian fit), rough estimates were made to find the peak position corresponding to the secondary star. It can be theorized that the deblending method is more accurate than the Gaussian profile fit. This is because the latter recalculates the peak positions by considering the distribution of data points within the region in which blending appears, where as the former accepts the rough estimates of peak positions marked manually.

Another difficulty arose when using the broadening function technique because the IDL software produced somewhat unacceptable results. It was reasoned by Rucinski that this could be due to the fact that H- alpha line is filled with emissions and greatly broadened and the IDL software is sensitive to such phenomena. Therefore it was suggested that the broadening function technique be used for emission free metallic lines.

**Interpretation of results:** The most recent spectroscopic studies on this binary system were made by Rucinski & Duerbeck in 2006 using the Broadening Function method. The only previous spectroscopic observations were by Popper (1956) who saw only the bright component with the amplitude of the velocity curve  $k_1 = 92.3 \pm 1.5$  km/s. In contrast, Rucinski & Duerbeck have detected the secondary component in the broadening functions.

The velocity curves obtained in our study, using both Gaussian profile fit and deblending methods agrees with that of Rucinski and Duerbeck to a great extent. From the velocity curve obtained for H-alpha line spectroscopic data, the calculated orbital velocities of the primary and secondary components are  $v_1 = 89.261$  kms<sup>-1</sup> and  $v_2 = 208.589$  kms<sup>-1</sup> respectively.

Popper from his data derived the photometric mass ratio  $q_{\text{phot}} = 0.59 \pm 0.02$  and Rucinski and Duerbeck found from their spectroscopic data that  $q_{\text{sp}} = 0.33 \pm 0.02$ . The spectroscopic mass ratio calculated using the data obtained in this study,  $q_{\text{sp}} = 0.42 \pm 0.09$ .

In this study we have noticed that the radial velocity curve obtained from H alpha line profiles of the primary component show positive velocity values for phases from 0 to 0.25. This is a clear deviation from what is expected because theoretically negative velocity values must result between phases 0 and 0.5. Therefore when obtaining the radial velocity curves only the data points of the phases from 0.5 to 1 were accepted. Assuming the radial velocity curve to be symmetrical as seen in the previous studies on this system the velocity curve was extrapolated to phases from 0 to 0.5.

Additional absorption line profiles of Fe and Al metals were obtained later during the month of May in order to verify the extrapolated values obtained from phase 0 to 0.5 of H alpha line profiles. A greater exposure time (20 minutes) were used for each spectrum as these lines are weaker than the H alpha line. At the time of taking these spectra S Ant was visible only for a short period as it was setting very early. Therefore we were able to take spectra of phases from phases 0.1-0.3. From the velocity curve obtained for these set of data we have calculated the amplitude of the primary component  $k_1 = 74$  kms<sup>-1</sup> which is very close to the value  $77.84$  kms<sup>-1</sup> obtained by Slavek M. Rucinski and Hilmar W. Duerbeck (2006)

The metallic line profiles also suggest that the reason for positive velocity values of the profiles of the primary component was indeed due to a phenomenon connected with the H-alpha line of spectra. The Hydrogen gas stream in the envelop of this contact binary system, seen within this phase and moving away from us could have caused the positive radial velocity values.

## List of references

- Ruccinski, S.M., Duerbeck, H.W. : 2006, Radial Velocity Studies of Southern Close Binary Stars. II. Spring/Summer Systems1
- Ruccinski, S.M.: 2002, Radial Velocity Studies of Southern Close Binary Stars. Methods and Uncertainties
- Ruzzo, G., Sollazzo, C., Maceroni, C., Milano, L. : 1981, Determination of parameters of W Uma systems
- Popper, D.M. :1957, Photoelectric Observations of Eclipsing Binaries.
- Durasevic, G. :1997, An Analysis of the Light Curves of The Active Close Binary SW Lac
- Barnes, J.: 1993, A Beginner's Guide to Using IRAF-IRAF Version 2.10
- Erika,B.V.: 1989, Introduction to Stellar Astrophysics, *Volume 1*, pp 67-87, Cambridge University Press.
- Emerson, D: 1996, Interpreting Astronomical Spectra, John Wiley and sons

## Websites

[http://adsabs.harvard.edu/ads\\_abstracts.html](http://adsabs.harvard.edu/ads_abstracts.html)

<http://simbad.u-strasbg.fr/simbad/>

[www.astro.uiuc.edu](http://www.astro.uiuc.edu)

[www.optec.com](http://www.optec.com)

[www.iraf.noao.edu](http://www.iraf.noao.edu)

[www.sbgj.com](http://www.sbgj.com)

# APPENDIX

Table 6.1 Phase calculation of observed spectra of S Ant

OBS DATE (DATE)	OBS TIME (LOCAL)	JULIAN DATE	HEL. JUL. DATE	CORRECTION	PHASE
21-Jan-07	1:11:30	2454121.32048611	2454121.323992	5.048863	0.60630
21-Jan-07	1:39:38	2454121.34002315	2454121.343530	5.050185	0.63644
21-Jan-07	1:55:45	2454121.35121528	2454121.354723	5.050943	0.65370
21-Jan-07	2:09:31	2454121.36077546	2454121.364284	5.051589	0.66844
21-Jan-07	2:23:08	2454121.37023148	2454121.373740	5.052228	0.68303
21-Jan-07	2:42:36	2454121.38375000	2454121.387259	5.053142	0.70388
21-Jan-07	2:57:16	2454121.39393519	2454121.397445	5.053830	0.71959
21-Jan-07	3:19:40	2454121.40949074	2454121.413001	5.054881	0.74359
21-Jan-07	3:34:19	2454121.41966435	2454121.423175	5.055568	0.75928
21-Jan-07	3:48:19	2454121.42938657	2454121.432898	5.056225	0.77427
21-Jan-07	4:03:33	2454121.43996528	2454121.443477	5.056939	0.79059
21-Jan-07	4:18:32	2454121.45037037	2454121.453883	5.057641	0.80664
21-Jan-07	4:32:31	2454121.46008102	2454121.463594	5.058296	0.82162
21-Jan-07	4:47:08	2454121.47023148	2454121.473745	5.058981	0.83728
21-Jan-07	5:04:42	2454121.48243056	2454121.485944	5.059803	0.85609
21-Jan-07	5:18:43	2454121.49216435	2454121.495679	5.060460	0.87111
21-Jan-07	5:33:23	2454121.50234954	2454121.505864	5.061146	0.88682
23-Jan-07	0:30:59	2454123.29234954	2454123.295946	5.179181	0.64781
23-Jan-07	1:10:04	2454123.31949074	2454123.323089	5.180930	0.68968
23-Jan-07	1:51:55	2454123.34855324	2454123.352152	5.182802	0.73451
23-Jan-07	2:04:50	2454123.35752315	2454123.361123	5.183380	0.74834
23-Jan-07	2:17:25	2454123.36626157	2454123.369862	5.183942	0.76182
23-Jan-07	2:35:36	2454123.37888889	2454123.382489	5.184755	0.78130
23-Jan-07	3:08:32	2454123.40175926	2454123.405361	5.186225	0.81657
23-Jan-07	3:22:14	2454123.41127315	2454123.414875	5.186837	0.83125
23-Jan-07	3:34:45	2454123.41996528	2454123.423568	5.187396	0.84466
23-Jan-07	3:47:07	2454123.42855324	2454123.432156	5.187948	0.85790
23-Jan-07	4:02:32	2454123.43925926	2454123.442862	5.188636	0.87442
23-Jan-07	4:15:26	2454123.44821759	2454123.451821	5.189211	0.88823
23-Jan-07	4:28:11	2454123.45707176	2454123.460676	5.189780	0.90189
23-Jan-07	4:41:04	2454123.46601852	2454123.469623	5.190354	0.91569
23-Jan-07	5:00:25	2454123.47945602	2454123.483061	5.191216	0.93642
23-Jan-07	5:15:32	2454123.48995370	2454123.493559	5.191890	0.95261
23-Jan-07	5:29:45	2454123.49982639	2454123.503432	5.192523	0.96784
31-Jan-07	21:08:54	2454132.15201389	2454132.155961	5.683709	0.31338
31-Jan-07	21:59:44	2454132.18731481	2454132.191263	5.685444	0.36783
31-Jan-07	23:40:14	2454132.25710648	2454132.261057	5.688868	0.47548
1-Feb-07	0:15:11	2454132.28137731	2454132.285329	5.690057	0.51292
1-Feb-07	1:02:01	2454132.31390046	2454132.317853	5.691648	0.56308
1-Feb-07	1:16:31	2454132.32396991	2454132.327923	5.692141	0.57861
9-Feb-07	22:23:08	2454141.20356481	2454141.207769	6.053683	0.27476
9-Feb-07	23:36:44	2454141.25467593	2454141.258881	6.055336	0.35360
10-Feb-07	0:02:57	2454141.27288194	2454141.277087	6.055924	0.38168
10-Feb-07	1:37:47	2454141.33873843	2454141.342945	6.058046	0.48326
10-Feb-07	2:32:41	2454141.37686343	2454141.381071	6.059270	0.54206
10-Feb-07	2:50:10	2454141.38900463	2454141.393213	6.059659	0.56079

10-Feb-07	3:10:59	2454141.40346065	2454141.407669	6.060122	0.58309
10-Feb-07	3:26:20	2454141.41412037	2454141.418329	6.060463	0.59953
10-Feb-07	3:41:47	2454141.42484954	2454141.429058	6.060807	0.61608
10-Feb-07	4:05:11	2454141.44109954	2454141.445309	6.061326	0.64114
10-Feb-07	5:22:47	2454141.49498843	2454141.499199	6.063045	0.72426
20-Feb-07	20:00:18	2454152.10437500	2454152.108745	6.292539	0.08828
20-Feb-07	20:25:46	2454152.12206019	2454152.126430	6.292740	0.11556
20-Feb-07	20:40:32	2454152.13231481	2454152.136685	6.292855	0.13138
20-Feb-07	20:52:24	2454152.14055556	2454152.144926	6.292948	0.14409
20-Feb-07	21:06:47	2454152.15054398	2454152.154914	6.293060	0.15949
20-Feb-07	21:20:19	2454152.15994213	2454152.164312	6.293166	0.17399
20-Feb-07	21:33:04	2454152.16879630	2454152.173167	6.293265	0.18764
20-Feb-07	21:47:10	2454152.17858796	2454152.182958	6.293375	0.20275
20-Feb-07	22:01:50	2454152.18877315	2454152.193144	6.293489	0.21846
20-Feb-07	22:23:38	2454152.20391204	2454152.208283	6.293657	0.24181
20-Feb-07	22:37:10	2454152.21331019	2454152.217681	6.293762	0.25630
20-Feb-07	23:07:34	2454152.23442130	2454152.238792	6.293996	0.28886
20-Feb-07	23:22:14	2454152.24460648	2454152.248977	6.294109	0.30457
20-Feb-07	23:35:12	2454152.25361111	2454152.257982	6.294208	0.31846
21-Feb-07	0:01:21	2454152.27177083	2454152.276142	6.294408	0.34647
21-Feb-07	0:15:46	2454152.28178241	2454152.286154	6.294518	0.36191
14-May-07	21:01:16	2454235.14671296	2454235.147772	1.524564	0.16654
14-May-07	22:17:50	2454235.19988426	2454235.200939	1.519067	0.24855
16-May-07	19:46:54	2454237.09506944	2454237.095988	1.322460	0.17144
16-May-07	20:12:47	2454237.11304398	2454237.113961	1.320590	0.19916
16-May-07	20:50:47	2454237.13943287	2454237.140348	1.317843	0.23986
16-May-07	21:09:50	2454237.15266204	2454237.153576	1.316466	0.26027
16-May-07	21:24:31	2454237.16285880	2454237.163772	1.315405	0.27599
16-May-07	21:39:24	2454237.17319444	2454237.174107	1.314329	0.29193
16-May-07	21:58:08	2454237.18620370	2454237.187115	1.312975	0.31200
16-May-07	22:20:15	2454237.20156250	2454237.202473	1.311376	0.33568

## Error Analysis

	Gaussian Profile Fit	Deblending Method
	Error of measurement km/s	Error km/s
Primary Component	$\pm 19.91$	$\pm 6.67$
Secondary Component	$\pm 48.27$	$\pm 41.49$

$$\delta v_1 = 6.67 \quad \delta v_2 = 41.49$$

$$\text{spectroscopic mass ratio } r = \frac{v_1}{v_2}$$

$$(\delta r)^2 = \left( \frac{\partial r}{\partial v_1} \right)^2 (\delta v_1)^2 + \left( \frac{\partial r}{\partial v_2} \right)^2 (\delta v_2)^2$$

$$\delta r = \left[ \left( \frac{1}{v_2} \right)^2 6.67^2 + \left( \frac{v_1}{v_2^2} \right)^2 41.49^2 \right]^{\frac{1}{2}}$$

$$\delta r = 0.09$$

$$M_1 + M_2 = \frac{(v_1 + v_2)^3}{2\pi G} T, \quad M_2 = rM_1$$

$$(1+r)M_1 = \frac{(v_1 + v_2)^3}{2\pi G} T \Rightarrow M_1 = \frac{(v_1 + v_2)^3}{2\pi G(1+r)} T$$

$$(\delta M_1)^2 = \left( \frac{\partial M_1}{\partial r} \right)^2 (\delta r)^2 + \left( \frac{\partial M_1}{\partial v_1} \right)^2 (\delta v_1)^2 + \left( \frac{\partial M_1}{\partial v_2} \right)^2 (\delta v_2)^2 + \left( \frac{\partial M_1}{\partial T} \right)^2 (\delta T)^2$$

$$\delta M_1 = \left[ \left( \frac{(v_1 + v_2)^3}{2\pi G(1+r)^2} T \right)^2 (\delta r)^2 + \left( 3 \frac{(v_1 + v_2)^2}{2\pi G(1+r)} T \right)^2 (\delta v_1)^2 + \left( \frac{(v_1 + v_2)^2}{2\pi G(1+r)} T \right)^2 (\delta v_2)^2 + \left( \frac{(1+r)(v_1 + v_2)^3}{2\pi G} \right)^2 (\delta T)^2 \right]^{\frac{1}{2}}$$

$$\left(1 + \frac{1}{r}\right) M_2 = \frac{(v_1 + v_2)^3}{2\pi G} T \Rightarrow M_2 = \frac{(v_1 + v_2)^3}{2\pi G(1 + \frac{1}{r})} T$$

$$\delta M_2 = \left[ \left( \frac{(v_1 + v_2)^3}{2\pi G(1+r)^2} T \right)^2 (\delta r)^2 + \left( 3 \frac{(v_1 + v_2)^2}{2\pi G(1 + \frac{1}{r})} T \right)^2 (\delta v_1)^2 + \left( \frac{(1+r)(v_1 + v_2)^2}{2\pi G(1 + \frac{1}{r})} T \right)^2 (\delta v_2)^2 + \left( \frac{(1+r)(v_1 + v_2)^3}{2\pi G} \right)^2 (\delta T)^2 \right]^{\frac{1}{2}}$$